

ICEBERG STABILITY AND DETERIORATION

CENTRE FOR NEWFOUNDLAND STUDIES

**TOTAL OF 10 PAGES ONLY
MAY BE XEROXED**

(Without Author's Permission)

BO LIANG



INFORMATION TO USERS

This manuscript has been reproduced from the microfilm master. UMI films the text directly from the original or copy submitted. Thus, some thesis and dissertation copies are in typewriter face, while others may be from any type of computer printer.

The quality of this reproduction is dependent upon the quality of the copy submitted. Broken or indistinct print, colored or poor quality illustrations and photographs, print bleedthrough, substandard margins, and improper alignment can adversely affect reproduction.

In the unlikely event that the author did not send UMI a complete manuscript and there are missing pages, these will be noted. Also, if unauthorized copyright material had to be removed, a note will indicate the deletion.

Oversize materials (e.g., maps, drawings, charts) are reproduced by sectioning the original, beginning at the upper left-hand corner and continuing from left to right in equal sections with small overlaps.

ProQuest Information and Learning
300 North Zeeb Road, Ann Arbor, MI 48106-1346 USA
800-521-0600

UMI[®]



National Library
of Canada

Acquisitions and
Bibliographic Services

395 Wellington Street
Ottawa ON K1A 0N4
Canada

Bibliothèque nationale
du Canada

Acquisitions et
services bibliographiques

395, rue Wellington
Ottawa ON K1A 0N4
Canada

Your file Votre référence

Our file Notre référence

The author has granted a non-exclusive licence allowing the National Library of Canada to reproduce, loan, distribute or sell copies of this thesis in microform, paper or electronic formats.

The author retains ownership of the copyright in this thesis. Neither the thesis nor substantial extracts from it may be printed or otherwise reproduced without the author's permission.

L'auteur a accordé une licence non exclusive permettant à la Bibliothèque nationale du Canada de reproduire, prêter, distribuer ou vendre des copies de cette thèse sous la forme de microfiche/film, de reproduction sur papier ou sur format électronique.

L'auteur conserve la propriété du droit d'auteur qui protège cette thèse. Ni la thèse ni des extraits substantiels de celle-ci ne doivent être imprimés ou autrement reproduits sans son autorisation.

0-612-73608-3

Canada

ICEBERG STABILITY AND DETERIORATION

By

©Bo Liang, B.Eng.

**A thesis submitted to the School of Graduate
Studies in partial fulfillment of the
requirements for the degree of
Master of Engineering**

**Faculty of Engineering and applied Science
Memorial University of Newfoundland**

August 2001

St. John's

Newfoundland

Canada

Abstract

Icebergs pose unique risks to shipping and offshore oil and gas operations on the Grand Banks. These include risks of impact on fixed and floating installations, and risks of scour on sub-sea installations, such as pipelines and wellheads. Iceberg size, shape and stability are needed to determine the interactions and risks. A model is presented that focuses on the relationship between iceberg motion and its stability. Then melting and towing are considered separately. An example is shown to illustrate how changes in shape due to melting can lead to instabilities that result in the iceberg's reorientation to a new, more stable position. Meanwhile some other examples are shown to demonstrate how towing force and water drag force change the stability and motion of the iceberg. The work is a first step towards an iceberg evolution model that will eventually incorporate a detailed description of iceberg shape changes due to melting and fragmentation. Some of the consequences of reorientation, such as changes in draft and hydrostatic forces distribution, can then be considered. Such an iceberg evolution model will be a tool to aid iceberg risk assessment and iceberg management.

Acknowledgement

I would like to express my most sincere gratitude and appreciation to my supervisors Dr. Brian Veitch and Dr. Claude Daley, for their guidance throughout the research and the preparation of this thesis.

I would also like to express my sincere thanks to other professors in the faculty of Engineering at Memorial University of Newfoundland for many valuable discussions and useful suggestions.

Help from the technical staff at the Faculty of Engineering and Applied Science is gratefully acknowledged. Assistance of fellow graduate students is appreciated.

I also like to take this opportunity to acknowledge the financial support through my supervisors' research grant that made this work possible.

Finally, my dedication is due to my parents and my wife for their encouragement and support.

Table of Contents

Abstract	i
Acknowledgement	ii
Table of Contents	iii
List of Figures	vi
List of Tables.....	viii
List of Symbols	ix
Chapter 1 Introduction	1
1.1 Aim.....	1
1.2 Scope	2
Chapter 2 Literature Review	5
2.1 Ice thermodynamics	6
2.1.1 Surface melting due to insolation.....	6
2.1.2 Melting due to buoyant vertical convection	8
2.1.3 Melting due to forced (air and water) convection	12
2.1.4 Wave erosion.....	15
2.2 Deterioration Models.....	19
2.3 Iceberg Shape	27
2.4 Hydrostatics and Stability	30
2.4.1 Potential energy approach	30
2.4.2 Shape/Motion analysis approach.....	33
Chapter 3 Methods	38

3.1	Scope	38
3.2	Basic stability theory	38
3.3	Shape definition and coordinate system transformation	40
3.3.1	Shape definition.....	40
3.3.2	Coordinate system transformation: position, translation velocity, and force vectors	43
3.3.3	Coordinate system transformation: angular velocity vectors	47
3.4	Pressure integration technique	49
3.5	Volume and centre of mass	53
3.5.1	Volume of the ice model	53
3.5.2	Weight of the ice model	54
3.5.3	Centre of the buoyancy and centre of the mass.....	55
3.6	Water plane area.....	56
3.7	Properties of ice body.....	57
3.7.1	Moment of inertia and product of inertia	57
3.8	Coordinate system transformation in simulation	58
3.8.1	Initial transformation matrix	58
3.8.2	Simulation process	59
3.9	Equations of motion for a body moving with six degrees.....	60
3.9.1	Motion equations.....	60
3.9.2	Forces and moments.....	64
3.10	Coefficient selection.....	65
3.11	Simulation method	66
3.12	Potential energy map.....	66
3.13	Computer program design	67
3.13.1	Format of input file	69
3.13.2	Data structure of the model in the program.....	69
Chapter 4	Results and Discussion	71
4.1	Potential energy shapes map and motion simulation	72

4.2	Stability evaluation and simulation	77
4.3	Melting simulation	80
4.4	Towing simulation.....	82
4.5	Drift simulation	91
Chapter 5	Conclusions and Suggestions for Further Research	96
5.1	Conclusions	96
5.2	Suggestions for further research.....	97
References		99
Appendix A		103
A-1	Runge-Kutta method	103
Appendix B		106
B-1	Flow charts of the STABLE.....	106
	Main flow chart	106
	Statistical analysis section	107
	Potential energy analysis section.....	108
	Motion simulation section	109
	Towing and drag simulation section	110
Appendix C		111
C-1	A SLA format sample file	111

List of Figures

Figure 2-1 Iceberg surface melting rate due to insolation at 50°N latitude (after White et al., 1980).....	8
Figure 2-2 Three estimates of the convection melt rate of a nearly vertical ice surface...	12
Figure 2-3 Theoretical iceberg average melting rate due to forced convection, for various waterline length (after White et al., 1980).....	15
Figure 2-4 Computed wave erosion rate profiles for a smooth surface at $H=1m$ (after White et al. 1980)	18
Figure 2-5 The reduction of the iceberg's sea level horizontal area as a function of time (from Robe et al. 1977)	19
Figure 2-6 Effect of iceberg roughness on wave erosion (US Coast Guard, 2001)	23
Figure 2-7 Floating homogeneous body in dynamic equilibrium (from Bass and Peters, 1984).....	31
Figure 2-8 Vertical cross-section of a floating homogeneous body, shown in equilibrium and in a tilted position (from Bass, 1980)	34
Figure 3-1 Vertical cross-section of an icebrg	39
Figure 3-2 Body coordinate system	41
Figure 3-3 Space and body coordinate systems	42
Figure 3-4 Rotation of body axes through azimuth angle Ψ	44
Figure 3-5 Rotation of body axes through trim angle Θ	44
Figure 3-6 Rotation of body axes through roll angle Φ	45

Figure 3-7 Floating body equilibrium	52
Figure 3-8 User Interface of the STABLE program.	68
Figure 3-9 Data structure of the model in program.....	70
Figure 4-1 Stability simulation of a cone	73
Figure 4-2 Energy map of a cone	74
Figure 4-3 Energy map (close) of a cone	74
Figure 4-4 Stability simulation of an iceberg.....	75
Figure 4-5 Energy map of an iceberg.....	76
Figure 4-6 Energy map (close) of an iceberg.....	76
Figure 4-7 Real movement of an ice model compared with the simulation.....	79
Figure 4-8 Melting and stability simulation	81
Figure 4-9 Towing force F_T acted on the body at the water surface	83
Figure 4-10 Towing force acts above the centre of gravity	85
Figure 4-11 Towing force F_T acted on the body below the water surface	86
Figure 4-12 Towing force acts under the centre of gravity.....	87
Figure 4-13 Ice model rolls over	90
Figure 4-14 Water drag force acted on the body.....	92
Figure 4-15 Velocities of the iceberg in two situations	95

List of Tables

Table 2-1 Characteristic length of icebergs (US Coast Guard, 2001).....	20
Table 2-2 Deterioration caused by each process considered methods over one day assuming: Wave height=6ft, Wave period=10sec, and Relative Velocity=25cm/sec (US Coast Guard, 2001)	20
Table 2-3 IIP iceberg size categories (IIP website).....	28
Table 2-4 Average iceberg size (Venkatesh et al. (1988)).....	28
Table 2-5 IIP iceberg shape categories	29
Table 3-1 Normalizing factors (Bass & Sen, 1986)	65
Table 4-1 Drag coefficients of various 3-D geometrical shapes (from Hoerner, 1965) ...	93

List of Symbols

Ice thermodynamics:

FC	Forced convective melting factor
Fl	Failure length
H	Mean height of the wave
L	Maximum waterline length of the iceberg
L_c	Characteristic length of the appropriate size of iceberg
N_u	Nusselt number
$P_{Present-melt} \cdot P_{Previous-melt}$	Percent of the original length that has melted
P_r	Prandtl number
q_w	Heat transfer rate per unit area at the iceberg surface
R	Roughness height of the iceberg surface for a rough ice wall
R_r	Reynolds number
R_{rn}	Wave Reynolds number
$S_{relative}$	Relative speed of the iceberg with respect to the historical geostrophic current
S_{state}	Sea state
S_{∞}	Uniform far-field water salinity
t	Thickness of the overhanging slab
T	Mean period of the waves
T_c	Time to calve of an iceberg for a steady wave field
T_f	Freezing temperature
T_i	Far field water temperature
T_w	Water temperature
T_{∞}	Uniform far-field water temperature

V_{ms}	Surface melt rate due to insolation
V_{mb}	Melt rate due to buoyant vertical convection
V_{mf}	Melt rate due to forced convection
V_{me}	Iceberg wave erosion melt rate
V_{melt}	Iceberg total melt rate
Z_{time}	Units of days

Physical constants:

g	Acceleration due to gravity
k	Thermal conductivity of ice
ρ_i	Density of ice
ρ_w	Density of sea water
ν_w	Water kinematic viscosity
Γ	Latent heat of melting of ice

Ice model motion:

A_{jk}	Added-mass coefficients
A_{ns}	Cross section area of a n-side polygon shaped iceberg
A_w	Submerged cross sectional area in a vertical plane of the iceberg
B_{jk}	Damping coefficients
\overline{BG}	Distance between the buoyancy centre and mass centre
\overline{BM}	Distance between the buoyancy centre and metacentre
C_{jk}	Hydrostatic restoring coefficients
D_w	Drag coefficient in water
$E(\Theta, \Phi)$	Potential energy

$f = 2\Omega \sin \phi$	Coriolis vector
{ <i>Force</i> }	Force vector in the body system
F_A	Air drag force
F_B	Buoyancy force of the submerged iceberg
F_D	Water drag force
$(F_{D_x}, F_{D_y}, F_{D_z})$	Water drag force in x , y and z direction in space system
F_G	Weight of the iceberg
F_p	Pressure gradient force
F_R	Radiation force of surface waves
F_T	Towing force in space system
$(F_{T_x}, F_{T_y}, F_{T_z})$	Towing force in x , y and z direction in space system
(F_x, F_y, F_z)	Force vector in x , y and z direction in the space system
\overline{GM}	Distance between the mass centre and metacentre
$\hat{i}, \hat{j}, \hat{k}$	Unit vectors in x, y, z axes' directions
I	Area moment of inertia of the water-plane section of the body about the major axis
(I_{xx}, I_{yy}, I_{zz})	Moment of inertia of the ice model
(I_{xy}, I_{yz}, I_{zx})	Product of inertia of the ice model
M	Generalized mass matrix
M ⁻¹	Inverse generalized mass matrix
{ <i>Moment</i> }	Moment vector in the body system
$(M_{D_x}, M_{D_y}, M_{D_z})$	Moment due to water drag force in x , y and z direction in space system
M_{jk}	Components of the generalized mass matrix for the ice mass
M_T	Moment due to the towing force in space system

$(M_{T_x}, M_{T_y}, M_{T_z})$	Moment due to towing force in x, y and z direction in space system
(M_x, M_y, M_z)	Moment vector in x, y and z direction in the space system
\hat{n}	Unit normal vector acting into the body and is a function of position (x, y, z) .
P	Pressure of the water with respect to the free surface at any point (x, y, z) below the free surface
S_s	Submerged surface area of an iceberg
S_T	Total surface area of an iceberg
S_w	Water plane area
T_R	Angular velocity transformation matrix
T_R^{-1}	Inverse angular velocity transformation matrix
T_T	Position, translational velocity, and force vectors transformation matrix
T_T^{-1}	Inverse position, translational velocity, and force vectors transformation matrix
V	Volume of the iceberg
V_a	Above-water volume of the iceberg
V_b	Below-water volume of the iceberg
V_i	Iceberg velocity
V_w	Water velocity
$\{x_B, y_B, z_B\}^T$	Centre of the buoyancy
$\{x_G, y_G, z_G\}^T$	Centre of the mass
$\{x_O, y_O, z_O\}^T$	Space axes fixed at the free water surface
$\{x_I, y_I, z_I\}^T$	Body axes fixed with the ice model such that its origin coincides with the centre of mass

(η_1, η_2, η_3)	Translational displacements in the x , y , and z directions with respect to the origin
$(\dot{\eta}_1, \dot{\eta}_2, \dot{\eta}_3)$	Translational velocity vector in the x , y , and z directions
$(\ddot{\eta}_1, \ddot{\eta}_2, \ddot{\eta}_3)$	Apparent translational acceleration in the x , y , and z directions with respect to the origin
(η_4, η_5, η_6)	Angular displacements due to rotational motion about the x , y , and z axes
$(\dot{\eta}_4, \dot{\eta}_5, \dot{\eta}_6)$	Rotational velocity vector about the body system
$(\ddot{\eta}_4, \ddot{\eta}_5, \ddot{\eta}_6)$	Rotational acceleration vector about the body system
(Φ, Θ, Ψ)	Eulerian angles describing the orientation of a body axes system in the space system. Yaw, pitch and roll respectively

Chapter 1

Introduction

1.1 Aim

The main aim of this thesis is to provide a method for the evaluation of the stability of an arbitrarily shaped iceberg. The changes in stability of an iceberg are mainly derived from two sources. One source is external forces, such as towing, wind, waves and currents. The other is shape change, due to melting and fragmentation. A numerical iceberg evolution model is developed here that simulates the stability, floatation, and motion of an iceberg. Changes in shape due to melting are then considered. Further, the effects of a towing force are examined. The iceberg stability and evolution model will be a tool to aid iceberg risk assessment and iceberg management.

1.2 Scope

Icebergs off the east coast of Canada pose a unique hazard to shipping and petroleum development. The probability of iceberg collision is decisive in evaluations of feasibility for different types of offshore structures, such as detachable, fixed, or floating structures. In order to avoid collision, the icebergs are tracked, and their drift trajectories are predicted using iceberg drift models. If possible, icebergs are towed away. Icebergs whose keels touch and plough through (scour) the soft sediments of the seabed may crush and rupture seabed installations such as wellheads, anchors, mooring systems, pipelines, and telecommunication cables.

When studying iceberg drift, towing, grounding and scouring, the environmental factors and the mechanical properties of the iceberg itself should be considered. Among those factors, deterioration and stability are the key components to construct a more accurate iceberg drift model, or instruct iceberg towing. If significant mass is lost by an iceberg due to melting or calving, it can change the iceberg's characteristics. Further, it can lead to instability or change the iceberg's drift trajectory. In this situation, the resulting motion is sometimes unexpected. In order to handle this, an iceberg deterioration model should be incorporated into iceberg drift models. The tendency of icebergs to roll or heel over is well known, and so the potential hazards and difficulties of towing unstable icebergs may be significant. It follows that there is a need for accurate techniques for determining the stability of a towed iceberg.

According to the main aim of this thesis, it is clear that the focus of this research is not impact, drift prediction, or scouring loads, but rather the iceberg itself. Icebergs in the Newfoundland and Labrador offshore environment change rapidly as they migrate from northern latitudes, where they originate, to the latitudes around Newfoundland where they disappear. The changes are due to wave erosion and associated calving, natural and forced convective melting, solar radiation melting, and fragmentation due to thermal, hydrostatic, and motion induced stresses. The shape changes will result in changes to stability. Then the stability changes of an iceberg will lead to changes in orientation and floatation. They will also change the distribution of weight and buoyancy. As the orientation and floatation position of an iceberg define its boundary conditions and thereby control its deterioration totally, stability is an important point in modeling iceberg evolution.

In this thesis, a method is presented that can be used to evaluate the stability, floatation, and motion of an arbitrarily shaped iceberg. Changes in shape due to melting and external forces, such as towing force and water drag force, are then considered. Some examples are shown to illustrate how the method works. In order to model an evolving iceberg shape, a substantial effort is required to keep an accurate and adaptive mesh. This is foregone here in order to concentrate on the stability and motion issues.

In Chapter 2, a general review of the iceberg literature is presented. In order to simulate the motion and melting of an iceberg, we need to know all its properties, such as

shape, volume, density, centroid, and moments of inertia. These components and other important parameters, such as the iceberg's generalized mass matrix and the selection of coefficients, are the main subject of Chapter 3. A numerical simulation method is described in Chapter 4 and some simulation results are presented and discussed. Conclusions drawn from the work and suggestions for further research are shown in Chapter 5. There are three appendices. Appendix A shows the basis of the numerical methods used in the simulation. Appendix B describes the simulation program used in the work in detail. And a sample of input model file for the program is listed in Appendix C as a reference.

Chapter 2

Literature Review

In general, we can categorize iceberg deterioration as discrete or continuous. The melting processes are continuous and fragmentation processes are discrete. The focus of this thesis is on the motion of a freely floating iceberg, including the reorientation processes as stability changes due to melting or external forces, such as towing force and water drag force.

Considering an arbitrarily shaped 3-dimensional iceberg, three critical components govern the relationship between the melting and movement. They are; ice thermodynamics, the shape of the iceberg and the iceberg movement due to the change of stability. In this chapter, a survey of previous work on iceberg melting, iceberg shape and iceberg stability is presented. At the end of this chapter, several iceberg deterioration models are also reviewed.

2.1 Ice thermodynamics

The deterioration of an iceberg is influenced mainly by five different processes (White et al., 1980, El-Tahan et al., 1987, Hanson, 1990). They are:

- Surface melting due to insolation.
- Melting due to buoyant vertical convection.
- Melting due to forced (air and water) convection.
- Wave erosion.
- Calving of overhanging ice, thermal stresses, 'faults' and wave induced stresses.

Because the continuous deterioration processes are the emphases of this review, the first four processes are considered here.

2.1.1 Surface melting due to insolation

Solar radiation on an iceberg surface is a minor but steady cause of mass loss from an iceberg, especially in the summer months. Figure 2-1 shows De Jong's (1973) values of measured insolation for the center of the Labrador Sea (60° N) and for the waters east of Newfoundland (50° N). In Figure 2-1, it can be seen that the more northerly point, being

less foggy than Newfoundland, reaches the maximum insolation ratio at about 50%. Latitude (incidence angle with the sun), roughness of the iceberg's surface, amount of bubble content, snow or frost cover, and local meteorological conditions, such as fog and cloud cover, are the key factors that affect the insolation on an iceberg. This is the reason the measured values of ice insolation ratios in the literature vary from less than 10% (clear, flat ice surface) to 60% (bubbly, frosted ice). Hobbs (1974) suggests 60% as representative of Arctic ice, but De Jong (1973) and Budyko (1972) suggest 30% to 40% as a mean value for sea ice.

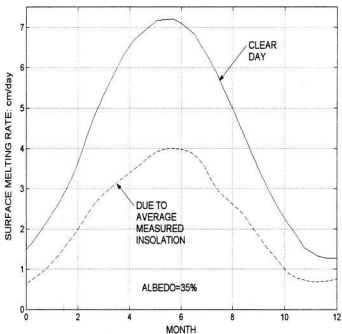


Figure 2-1 Iceberg surface melting rate due to insolation at 50°N latitude (after White et al., 1980)

2.1.2 Melting due to buoyant vertical convection

Buoyant vertical convection is the result of temperature and salinity differences between the iceberg melt water and the seawater. When ice melts in seawater, melting at the ice/water interface cools and dilutes the adjacent seawater. Because salinity effects dominate temperature effects on density, a region of positively buoyant water is created next to the ice wall that results in an upward flow. Further from the ice the salinity

quickly rises to its ambient value, but because of the comparatively larger thermal diffusivity from the ice to the water, the temperature remains depressed. This cold water of ambient salinity is negatively buoyant and sinks. Therefore, the complete flow field consists of an inner upward-flowing boundary layer that becomes thicker in the upward direction, and an outer downward-flowing boundary layer that becomes thicker in the downward direction. Thus, thermal buoyancy will be downward and saline buoyancy will be upward. Estimates of the net effect have been made by several authors.

Josberger (1977) used experimental and theoretical studies to estimate the buoyant convective melting rate. The experiment looked at a freshwater ice wall melting in salt water of uniform far-field temperature T_{∞} and salinity S_{∞} . Fieldwork was also done to validate the laboratory work. In the experiment, three different flow regimes were observed. There was a region of laminar flow at the bottom of the ice and one of turbulent flow farther up the ice wall. The two regions were separated by a zone of transition from laminar to turbulent flow. The interface temperature was observed to be dependent on flow regime. The coldest temperature occurred at the bottom of the laminar region and slowly increased with height until the turbulent region was encountered. In the turbulent region the interface temperature remained uniform and warmer than the ice wall temperature outside the turbulent region. The melting rate, measured normal to the surface of the ice wall, also depended on flow region. In the laminar regime, the greatest melt rate was found at the bottom of the ice wall, and decreased with increasing height from the bottom. The highest melt rates were found in the region of transition from

laminar to turbulent flow. The author also found that the ice face was smooth in the turbulent zone, and the melt rates in such zone were about 30% higher than in the laminar zone.

A field study was carried out to compare with the laboratory work. In this field measurement program, an iceberg with a waterline length of 100m, a height of 30m and a draft of 100m was examined. Based on the results derived from the lab experiment, the author estimated the melt rate of the iceberg was $0.1\text{m}\cdot\text{day}^{-1}$ and the boundary layer thickness was of the order 0.5m in the water with the temperature of $+2.0^{\circ}\text{C}$ and salinity of 33.0‰.

The melt rate equation obtained from the lab studies is given by

$$V_{mb} = 3.7 \times 10^{-2} (T_i - T_f)^{1.5} \text{m} \cdot \text{day}^{-1} \quad (2.1)$$

where V_{mb} is the melt rate due to buoyant vertical convection; T_i is the far field water temperature; and T_f is the freezing temperature.

Russell-Head (1980) observed ice blocks melting in water of different temperatures and salinities. The author examined the dependence of melt rate on salinity, water temperature and ice block size. From the experiment results, the author found that the

melting mode in fresh water was different from in water of sea-salinity, and if the salinity of water was between 17.5‰ and 35.0‰, the effect of salinity on the melt rates was insignificant. The bottom and side melt rates were similar, and the bottom melt rates were independent on the size of the ice block. Conversely, the side melt rate of the large block was lower than that of the medium block due to the greater thickness of the melt plume next to the large block.

From Russell-Head's study, a power relationship between the melt rate and temperature difference between the water temperature and the temperature at the onset of freezing of seawater (-1.8°C) can be denoted as

$$V_{mb} = 1.8 \times 10^{-2} (T_i + 1.8)^{1.5} \text{ m} \cdot \text{day}^{-1} \quad (2.2)$$

The third estimate of melt rate was given by Neshyba and Josberger (1979). The authors' work was based on Morgan and Budd's (1977) analysis of Antarctic iceberg size and latitude distributions. They fitted Morgan and Budd's eight data points to a least-squares parabola and subtracted the constant intercept as a "calving wastage". Finally, they arrived at the following estimate of vertical buoyant melt rates:

$$V_{mb} = 0.007616(T_i - T_f) + 0.0012877(T_i - T_f)^2 \text{ m} \cdot \text{day}^{-1} \quad (2.3)$$

All of these three melt rate estimates are plotted in Figure 2-2. From the picture, we can find that these three estimates differ substantially. Especially at higher temperature gradients, the estimated melt rates differ more and more. The differences in the experimental conditions, the scale factors between the model and the real iceberg, and the effect of the waves and current in the tanks lead to such big differences.

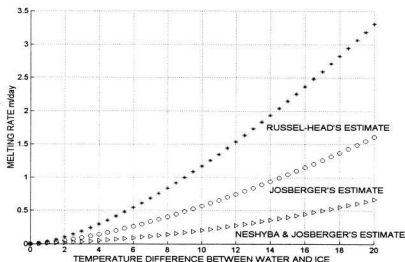


Figure 2-2 Three estimates of the convection melt rate of a nearly vertical ice surface

2.1.3 Melting due to forced (air and water) convection

The theory of forced convection iceberg melting is quite complex, as shown in a theory by Griffin (1977). If the icebergs are relatively small and the wind-driven relative

velocities are relatively strong, such as 10 to 30cm/s, the melt rates of icebergs from forced convection are significantly larger (about 6 times) than those from natural buoyant convection (White et al., 1980). In this situation, melting due to forced convection (wind) can be expected to be more important. When the wind speeds are very small or negligible, we can ignore the effect of the wind, and consider the melting due to forced convection to be largely dependent on the relative velocity and temperature of the water and ice. Even if atmospheric pressure gradient effects are neglected, a thick velocity boundary layer will be generated when the flow passes an iceberg. Because of the existence of this thick layer, the temperature of the ice wall varies according to salinity intrusion at the melt interface. An approximate means of evaluating the melt rates of tabular and non-tabular icebergs was developed by White et al. (1980).

$$V_{mf} = \frac{q_s}{\rho_i \Gamma} \quad (2.4)$$

where V_{mf} is melt rate due to forced convection, ρ_i is the density of ice, Γ is the latent heat of melting of ice, and the heat transfer rate per unit area at the iceberg surface, q_s , is denoted as

$$q_s = \frac{N_s \times k \times T_s}{L} \quad (2.5)$$

where T_w is the water temperature, k is the thermal conductivity, and L is the maximum waterline length.

The Nusselt number N_u can be written approximately for non-tabular icebergs and tabular icebergs as

$$\begin{aligned} N_u &= 0.055 R_r^{0.5} P_r^{0.4} && \text{non-tabular} \\ N_u &= 0.058 R_r^{0.5} P_r^{0.4} && \text{tabular} \end{aligned} \quad (2.6)$$

where R_r and P_r are the Reynolds and Prandtl numbers, respectively.

The melting rates from Eqn. (2.6) are plotted in Figure 2-3 for various iceberg lengths. From Figure 2-3, it is noticeable that the average melt rates for non-tabular icebergs and tabular icebergs differ only about 5%.

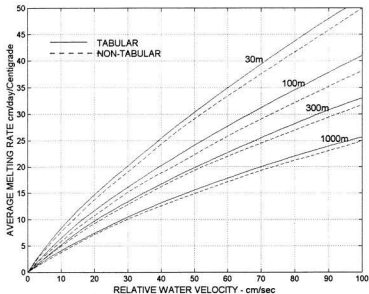


Figure 2-3 Theoretical iceberg average melting rate due to forced convection, for various waterline length (after White et al., 1980)

2.1.4 Wave erosion

Based on observations and laboratory experiments, we know that most of the melting of an iceberg takes place on its submerged surfaces. Wave erosion at the water line of the iceberg is the most important of the various mechanisms affecting iceberg deterioration. It is clear from published observations of icebergs (e.g., Groen 1969) that waves, even in cold waters, can rapidly erode a notch or ledge into the side of an iceberg, after which calving or fracture can occur. In the summer months, wave erosion and calving may together account for over 80% of iceberg mass loss.

Laboratory experiments on wave erosion of icebergs are few. In 1977, Josberger examined the effect of small flapper-generated waves with a height of 5 cm and a period of 0.4 sec on a vertical ice sheet in fresh water with a temperature of 4°C. A waterline notch of 8 cm deep was carved by the waves in 45 minutes. The notch extended in the vertical direction, one wave height notch above the waterline and about $\frac{1}{k}$ below the waterline, where k is wave number.

El-Tahan et al. (1987) observed that a sea state of 1 to 2 caused 0.5 to 1 m of erosion per day. Based on this observation, Bigg et al. (1997) extrapolated an approximate melt rate equation that was denoted by

$$V_{mw} = 0.5S_{state} \quad (2.7)$$

where V_{mw} is the iceberg wave erosion melt rate, and S_{state} is the sea state, calculated as a function of wind speed according to the marine Beaufort scale (Meteorological Office, 1969).

White et al. (1980) developed theoretical estimates of the amount of ice melted by wave action. The coefficients of their model were selected based on the comparison to Josberger's results and their own tests. They suggested that the iceberg wave erosion melt rate V_{mw} per degree Celsius of water temperature was a function of the mean height H

and period T of the waves, and the roughness height R of the iceberg surface for a rough ice wall. For a smooth ice wall, V_{ms} could be calculated in terms of the wave Reynolds number

$$R_{ts} = \frac{H^2}{T\nu_w} \quad (2.8)$$

where ν_w is the water kinematic viscosity.

The final correlations were given by

$$\begin{aligned} V_{ms} \times \frac{T}{H} &= 0.000146 \left(\frac{R}{H} \right)^{0.2} && \text{Rough wall} \\ V_{ms} \times \frac{T}{H} &= 0.00015 R_{ts}^{0.12} && \text{Smooth wall} \end{aligned} \quad (2.9)$$

where $\frac{R}{H}$ is the roughness ratio.

The smooth wall melt rates are plotted in Figure 2-4 for typical Reynolds numbers.

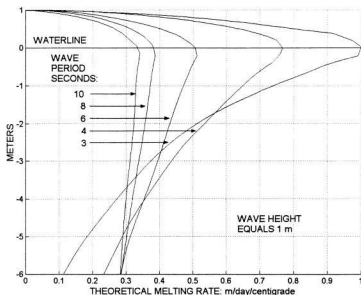


Figure 2-4 Computed wave erosion rate profiles for a smooth surface at $H=1\text{m}$ (after White et al. 1980)

Robe and Maier (1977) reported another excellent wave erosion example. In their report, a unique series of five photos taken of the same iceberg over a period of 25 days, from 12 May to 6 June 1976, was presented. In general, icebergs normally change their shape so rapidly by a combination of calving, melting and rolling, that it is hard to identify them after only a few days. In this case, the iceberg had only 4m to 5m of freeboard and stayed in a very stable position. In those 25 days, the iceberg decreased in surface area from approximately $190,000\text{m}^2$ to an area of $109,000\text{m}^2$. The rate of decrease in surface area due to wave erosion, undercutting and minor calving, was nearly linear (Shown in Figure 2-5).

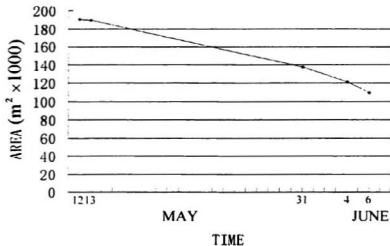


Figure 2-5 The reduction of the iceberg's sea level horizontal area as a function of time (from Robe et al. 1977)

2.2 Deterioration Models

In general, the population, stability and size distribution of icebergs are largely dependent on their deterioration rates. Several deterioration models have been developed in the past few decades (IIP, El-Tahan et al. (1984), Venkatesh et al. (1994), Venkatesh et al. (1985), Diemand et al. (1986)). One of the main aims of the models has been to have a way to predict gross changes in iceberg size over a period of days, to fill in the gaps between visual (aircraft) sightings. Many environmental parameters such as wind direction and speed, currents, waves, air and water temperatures were incorporated into some sophisticated models to obtain more accurate results. In this section, several models are reviewed.

The International Ice Patrol (IIP)'s deterioration model is based on White et al.'s report (1980). In this model, some of the physics, especially the continuous deterioration processes, such as buoyant convective, wind forced convective, insolation, and wave erosion melting were considered. The discrete deterioration processes, such as fragmentation and calving, were not included in the model. In order to make use of the equations in White et al.'s report, some associated environmental information, such as sea surface temperature (SST), wave height, and wave period, have to be obtained. The output from the deterioration model is presented in a simple form that gives the percentage of the original length that has been melted by the model. According to the requirement of IIP's model, each size of iceberg is assigned a characteristic length (Table 2-1). Four melting processes are discussed below in order of increasing importance (Table 2-2).

Table 2-1 Characteristic length of icebergs (US Coast Guard, 2001)

SIZE	CHARACTERISTIC LENGTH
Growler	16 meters
Small Iceberg	60 meters
Medium Iceberg	122 meters
Large Iceberg	225 meters

Table 2-2 Deterioration caused by each process considered methods over one day assuming: Wave height=6ft, Wave period=10sec, and Relative Velocity=25cm/sec (US Coast Guard, 2001)

MELTING CAUSED BY	DETERIORATION	% OF TOTAL
-------------------	---------------	------------

Insolation	0.02m/day	0.30%
Buoyant Convection	0.12m/day	1.60%
Forced Convection	0.93m/day	14.2%
Wave Induced	6.55m/day	84.0%

The equations used to estimate melting due to forced convection are based on Figure 2-3 (White et al., 1980). Because there is a change in the slope of the linear approximation at a relative velocity of about 25 cm/sec, the estimation equations were divided into two parts, one for relative speed less than 25 cm/sec and the other for greater than 25 cm/sec. The forced convective melting factor (FC) is written as

$$\begin{aligned}
 FC &= (0.934 - (0.202 \log_{10} L) S_{relative}) \text{ (cm/day/}^{\circ}\text{C) less than 25cm/sec} \\
 FC &= (0.660 - (0.151 \log_{10} L))(S_{relative} - 25) + (0.934 - (0.202 \log_{10} L))25 \quad (2.10) \\
 &\quad \text{(cm/day/}^{\circ}\text{C) greater than 25cm/sec}
 \end{aligned}$$

where L is the present waterline length of the iceberg, and $S_{relative}$ is the relative speed of the iceberg with respect to the historical geostrophic current. Using FC we can obtain the amount of deterioration due to forced convection:

$$V_{mf} = \frac{FC \cdot (T_i - T_f) \cdot Z_{ice} \cdot \frac{1}{2}}{100} \text{ cm / day} \quad (2.11)$$

where Z_{wave} is in units of half days (hence the 0.5) and the factor of 100 converts centimetres to meters.

The wave erosion is the most important component of iceberg deterioration (as shown in Table 2-2). The equation (2.9) is used to model the wave erosion. This equation is solved for melting rate due to wave erosion in meters per day (IIP):

$$V_{me} = \frac{H \cdot 0.000146 \cdot (2.0/H)^{0.2} \cdot 24 \cdot 3600 \cdot Z_{wave} \cdot 0.5 \cdot (T_i - T_f)}{100} \text{ m} \cdot \text{day}^{-1} \quad (2.12)$$

In order to use this equation, we should first assume a value for the roughness on the iceberg wall. The relationship between the iceberg roughness and the roughness factor is shown in Figure 2-6. In this model, a value of 2.0 cm was chosen.

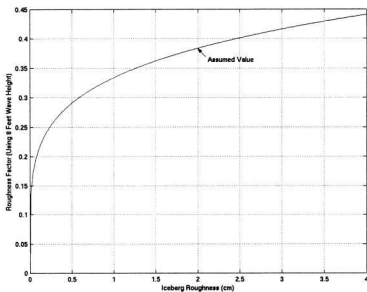


Figure 2-6 Effect of iceberg roughness on wave erosion (US Coast Guard, 2001)

The total melt V_{melt} for a given time period is calculated as:

$$V_{melt} = V_{mb} + V_{mf} + V_{mw} + V_{ms} \quad (2.13)$$

The final output (the percentage of the original length that has been melted by the model) for the time period between the present $P_{Present-melt}$ and the previous $P_{Previous-melt}$ can be calculated:

$$P_{Present-melt} = P_{Previous-melt} + \frac{V}{L_c} \cdot 100\% \quad (2.14)$$

where L_c is the characteristic length of the appropriate size of iceberg, and $P_{Previous-melt}$, $P_{Present-melt}$ are the percent of the original length that has melted.

El-Tahan et al. (1984) proposed a deterioration model, which was also based on White et al.'s report (1980). The model was used by the authors to simulate the deterioration of three icebergs in the Grand Banks/Labrador Sea off the Canadian east coast. Then the simulation results were compared with the observations. In their model, five deterioration processes were considered. They were; surface melt due to insolation, melting due to buoyant vertical convection, melting due to forced (air and water) convection, wave erosion, and calving of overhanging ice slabs. Except for the last process, the estimation equations adopted in the model were the same as the IIP's model. Considering the fragmentation process, White et al. (1980) pointed out that the failure length, Fl , could be estimated from

$$Fl = 0.33(37.5H + t^3)^{\frac{1}{2}} \quad (2.15)$$

where H is the wave height and t is the thickness of the overhanging slab. For a steady wave field, the time to calve, T_c , can be calculated based on the waterline erosion rate V_{mw} .

$$T_c = \frac{Fl}{V_{mw}} \quad (2.16)$$

It is notable that calving time decreases significantly with increasing wave height and decreasing wave period. The authors validate the simulation results with some field data. Three icebergs were involved in comparison. In the first case, the observation data of an iceberg reported by Kollmeyer (1965) was used. The authors found that the model simulations underestimated the mass loss by about 25% over the observation period. The authors believed that there were two reasons that could lead to the underestimation. One is the model did not account for mass loss resulting from calving induced by thermal stresses, and the other was errors in the estimates of the observed wave heights and period. In the other two cases, an iceberg reported by Robe et al. (1977) and an iceberg (iceberg No. 032, observed at Ogmund E-72 (1980), an offshore Labrador iceberg surveillance program), the predicted mass losses were in good agreement with the observed mass losses.

Venkatesh et al. (1993) examined two icebergs with their deterioration model. The authors mainly considered wave erosion and calving - two deterioration processes that

accounted for nearly 80% of the deterioration rate. The estimation equations used in their model were also based on White et al.'s report (1980). Unlike El-Tahan et al.'s model (1987), the authors found that the calving events were well simulated. Meanwhile the deterioration of icebergs as they emerged out of sea ice could be successfully modelled.

Venkatesh et al. (1985) reported a field study on the deterioration of two icebergs grounded outside St. John's harbour. A lot of data, such as berg-related, meteorological and oceanographic data, were collected during the period of 10-25 June 1983. The authors also compared the observation data with the simulation data. In their comparison, the deterioration model carried out by El-Tahan et al. (1984) was adopted. The mass losses due to insolation, buoyant vertical convection, forced convection in air and water, wave erosion and calving were simulated. The final conclusion was similar to the result of El-Tahan et al. (1984). For one case, the predicted mass loss underestimated by 10% with the observed mass loss. For the other case, the difference between the predicted and observed mass loss rates was about 30%. The authors explained this great difference in the same way as El-Tahan et al. (1984). The main reason was that the model could not simulate calving correctly. Compared with Table 2-2 pointed out in IIP's model, the simulation supported the opinion that wave erosion and calving may together account for over 80% of iceberg mass loss.

Diemand et al. (1986) approached the deterioration modelling in a different way. The authors divided the studies of the deterioration of icebergs into three categories. The first

was laboratory model tests in which melting phenomena involved in the ablation process were studied. The second was large-scale statistical studies on iceberg populations. The last was theoretical studies of calving of icebergs and glaciers based on known mechanical and materials properties of ice. The authors focused on the construction of a statistical model, and developed a simple Monte Carlo model to simulate the iceberg deterioration. In their model, icebergs could be selected from an initial mass distribution, and mass loss was assumed to be proportional to the product of a series of environmental factors.

2.3 Iceberg Shape

There are two widely used kinds of iceberg size and shape classification: one is defined by the IIP, and the other one is defined by the World Meteorological Organization (WMO) (1970).

The WMO divides icebergs into three categories: icebergs, bergy bits, and growlers, based on the size of the icebergs. A massive piece of glacial ice whose above water volume, or sail, extends at least 5 m above the waterline and has a water plane area greater than 300 m² is defined as an iceberg. A bergy bit's sail extends between 1 m and 5 m above the waterline and has a water plane area of about 100 to 300 m². A growler has a sail that extends less than 1 m above the waterline and a water plane area of about 20 m².

The IIP has two classifications, one is based on size, and the other one is based on shape. The size classification is shown in Table 2-3. Venkatesh et al. (1988) extended the size categories with more details, such as estimates of perimeter, mass, and surface area (shown in Table 2-4). Some details of shape categories defined by the IIP are shown in Table 2-5.

Table 2-3 IIP iceberg size categories (IIP website)

Category	Height [m]	Length [m]
Growler	< 1	< 5
Bergy Bit	1-4	5-14
Small	5-15	15-60
Medium	16-45	61-122
Large	46-75	123-213
Very Large	> 75	> 213

Table 2-4 Average iceberg size (Venkatesh et al. (1988))

Category	Length [m]	Mass (tonnes)	Perimeter [m]	Wetted surface area [m ²]	Total surface area [m ²]
Growler (non tabular)	10	450	30	250	350
Small (non tabular)	55	75,000	155	8,000	10,300
Medium (non tabular)	125	900,000	360	36,000	48,000
Large (non tabular)	225	5,500,000	650	110,000	150,000
Small (tabular)	80	250,000	235	15,000	20,000
Medium (tabular)	175	2,170,000	500	67,000	92,000
Large (tabular)	260	8,230,000	750	150,000	204,000

Table 2-5 IIP iceberg shape categories

Category	Sub-category	Description	Ratio of water length to sail height
Tabular		Horizontal Or Flat tops	>5:1
Non tabular	Blocky	Steep sided And Flat topped	2.5:1
	Pinnacle	A central spire Or A pyramid shape that may has several pinnacles	NULL
	Dry dock	A wave eroded U-shape slot between two or more columns or pinnacles	NULL
	Dome	Smooth and rounded with low sides	NULL

A recent report (Anon, 1999), sponsored by the Program for Energy Research and Development (PERD), integrated three-dimensional shape and geometry for icebergs observed on the Grand Banks of Canada into a single database. The database collected the information of iceberg projects over the past 20 years, and contained dimensions for 872 icebergs, detailed 3-dimensional information for 28 iceberg keels as measured from sonar profiling, detailed 3-dimensional information for 566 iceberg sails as measured from stereo photography, and 2-dimensional profiles for 155 iceberg sails and keels.

Based on this database, an iceberg visualization project was developed by Barker et al. (1999). This project was also sponsored by the PERD. In this visualization database, 79 records that contained 3-dimensional data, in the form of x-y-z-coordinate data, could be used to provide an informative view of actual icebergs, in which showing keels for 25 icebergs, sails for 52 icebergs and complete shapes for 3 icebergs.

2.4 Hydrostatics and Stability

Several stability evaluation models have been reported in the literature. In general, two main methods have been used to study the stability of an iceberg. One is a potential energy approach and the other is a shape/motion analysis approach.

2.4.1 Potential energy approach

The potential energy method to analyse the stability of a floating body has been studied for several decades. In 1984, Bass and Peters developed an interactive computer program to analyse the position of equilibrium of a floating homogeneous body. In their method, the stability of that equilibrium position was determined by the relative vertical movements of centre of buoyancy B and centre of gravity G. The vertical distance of B from G is a measure of the potential energy. The horizontal distance between B and G, GZ, is defined as the lever arm of the gravity force and buoyancy (shown in Figure 2-7).

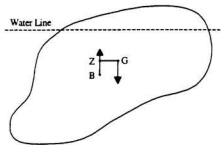


Figure 2-7 Floating homogeneous body in dynamic equilibrium (from Bass and Peters, 1984)

If the potential energy was at a minimum value, the iceberg is in a stable equilibrium position. If the lever arm GZ was equal to zero but the potential energy was not a minimum, the iceberg was in an unstable equilibrium position. If GZ was identically zero over some range of orientations, then the iceberg was said to be neutrally stable over that range. In such a situation, the potential energy was constant over a neutrally stable range. In their program, a 2-dimension model was divided into horizontal or vertical strips to calculate the gravity and buoyancy, and the centres of gravity and buoyancy. Finally, the relationship between righting lever and potential energy could be drawn. From such relationship, they focused on the draft changes when the iceberg sought the more stable position. In their work, they drew a conclusion that when an iceberg rolled from one orientation to another, it may increase its draft by as much as 50%, and an average for the increase in draft was approximately 25% for their 2-dimension models.

A potential energy method was also used to find the stable position of an iceberg by Lewis and Bennett (1984). The main aim of their study was to construct the relationship between rolling and draft changes. They generated model icebergs randomly, and calculated the potential energy as a function of angular displacement. Further, they calculated the draft changes when the model moved from a local minimum potential energy position to an absolute minimum one. The method the authors used is described as follows briefly.

In their paper, an iceberg was defined as a convex model, and its cross section was an n -sided polygon. To determine the potential energy for a given orientation, the iceberg was first rotated through the specified angle, about the centre of mass. The height of the waterline above the centre of mass was then adjusted using *Regula Falsi* method. Once the height of the waterline above the centre of mass of the iceberg had been found, the depth h_{cb} of the centre of buoyancy below the centre of mass could be calculated. Then the potential energy was given by

$$E = g\rho_i A_{iw} h_{cb} L \quad (2.17)$$

where A_{iw} was the area of the n -sided polygon, ρ_i was the density of the iceberg, g was the gravitational acceleration, and L was the length of the model iceberg in the direction of the axis of rotation. They examined 36,000 icebergs, and found that more than 25% of

those icebergs increased their drafts during rolling. Meanwhile, they pointed out that the majority of the changes were relatively minor, of the order of 10%.

Their model had several limitations and assumptions. First, the model icebergs were 2-dimensional, convex, and of constant, polygonal cross-section parallel to the axis of rotation. Second, the dynamics of roll were not included in their consideration.

2.4.2 Shape/Motion analysis approach

In 1980, Bass reported a study of the stability of icebergs. His study was much different from the potential energy method described above. He just considered the shape of the iceberg.

The basic theory the author adopted is shown in Figure 2-8. C is the centre of gravity of the portion of the iceberg above water, h_a is the height above the water line, B and G are the centre of buoyancy and the centre of gravity of the body, H_b is the depth below the water line, and M is the metacentre. The distance \overline{BM} can be written by the formula

$$\overline{BM} = \frac{I}{V_b} \quad (2.18)$$

where I is the area moment of inertia of the water-plane section of the body about the major axis and V_b is the below-water volume of the body. Furthermore, the distance \overline{GM} can be given as

$$\begin{aligned}\overline{GM} &= \overline{BM} - \overline{BG} \\ &= \frac{I}{7V_a} - 0.125(h_a + H_b)\end{aligned}\quad (2.19)$$

where V_a is the volume of the above-water portion of the berg. The only unknown (unless total information on the iceberg was available) is the value of H_b . Everything else may be calculated from the above-water portion.

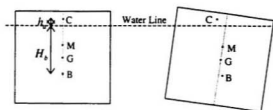


Figure 2-8 Vertical cross-section of a floating homogeneous body, shown in equilibrium and in a tilted position (from Bass, 1980)

To this end, three key parameters were introduced. The first one was the above-water fullness coefficient, and the second one was the under-water fullness coefficient, and the final one was the water-plane fullness coefficient. Using these three coefficients, the author defined a measured stability ratio, which was the ratio of average width to average height. If the measured stability ratio for a given iceberg with the above three coefficients was greater than the critical ratio, the iceberg was stable. Otherwise, it was unstable. In his paper, two simply shaped icebergs, the rectangular cubic model and the ellipsoidal model, were presented as examples. The author also examined a large number of iceberg types and gave their corresponding three fullness coefficients. The accuracy of his model depended greatly on the exact shape of an iceberg.

As an iceberg melts, the resulting change of shape can cause it to list gradually or to become unstable and topple over suddenly. Similarly, when an iceberg breaks up some of the individual pieces may capsize. Nye and Potter (1980) used Zeeman's analysis (Zeeman, 1977) of the stability of ships, which is based on Catastrophe theory, to analyse this problem. In their work, two concepts, metacentre and buoyancy centre, were replaced by metacentric locus and buoyancy locus. Together with the centre of gravity, one can find the equilibrium attitudes of the iceberg, whether they are stable or unstable, and whether a stable attitude is dangerously close to an unstable one. With the melting of the iceberg, the metacentric locus evolves. Its relation to the centre of gravity determines how the various equilibrium attitudes change and how attitudes of stable equilibrium might be destroyed. The main advantage of adopting catastrophe theory is that it gives a three-

dimensional geometrical picture that enables one to see all the possible equilibrium attitudes of a given iceberg, whether they are stable or unstable, whether a stable attitude is dangerously close to an unstable one, and how positions of stable equilibrium can be destroyed as the shape of the iceberg evolves with time. There are some weaknesses in catastrophe theory applied to iceberg analysis. The catastrophe theory modeling is more suited to analyze stability for a ship than for an iceberg. For a ship, metacentric locus is fixed while buoyancy locus is changeable. For an iceberg, both change. Catastrophe theory appears to predict a rectangular iceberg will heel to a small angle when it becomes unstable. In fact it rolls 90 degrees.

In Benedict's paper (1980), three modeling techniques were used to calculate the properties of an iceberg. Those properties included the centre of gravity, centre of buoyancy, above- and below-water volumes, mass, cross-sectional areas, and moments of inertia. The first technique was to fix a certain geometrical shape, which defined a class of objects whose individual members were defined by specifying one or more parameters, and to assume that the iceberg could be modelled as a member of this class. The second method was to use a "building block" approach, constructing the model by packing together a number of identical elements. The third one was to represent the iceberg surface as a series expansion in terms of analytic functions. In the first approach, the metacentre height was calculated and used to judge whether the iceberg was stable or not. In the second method, the author calculated the position of the centre of gravity and the centre of buoyancy. By comparing these two positions, one could determine whether the

iceberg was stable or not. In the function method, the author could compute the properties of the iceberg, and then analyse its stability.

All the models reviewed above share common features. First, all the studies deal with the 2-dimensional models. Second, the authors examined some selected simple shapes. Third, static conditions were considered in their models. Compared with dealing with the simple 2-dimensional shape, an arbitrarily shaped 3-dimensional model is much more complicated. More effort is required to compute the properties of the model. Further, the results derived from the static analysis are not comprehensive. For example, if we do not consider the inertia and motion of a model, it may stay in some local stable position. If the above factors are considered, the model may pass through a local stable position and move to another more stable one.

Chapter 3

Methods

3.1 Scope

Evaluation of the hydrostatic, floatation, and stability properties of an arbitrarily shaped floating body is not trivial. Some attempts have been made to set simple stability criteria for iceberg shapes using information that can be estimated from the above water portion of the iceberg (e.g. Weeks & Mellor 1977, Bass 1980). The approach taken here is based on integration of pressure over the elemental areas that make up the iceberg's surface (see e.g. Witz & Patel 1984 and Harrison, Patel & Witz 1989).

3.2 Basic stability theory

To start, basic stability theory for an iceberg will be reviewed briefly.

In Figure 3-1, G is the centre of gravity of the floating iceberg, and B is the centre of buoyancy. For a floating body, there are two hydrostatic conditions that govern the static position and orientation. The first, based on Archimedes Principle, is that the ratio of the underwater volume to the total volume must equal the ratio of the density of ice to that of seawater. That is to say, the weight of an iceberg must equal the buoyancy. The second is that the centre of gravity must be vertically in line with the centre of buoyancy. This means B and G should be on the same vertical line (Figure 3-1). Any iceberg should satisfy these two conditions.

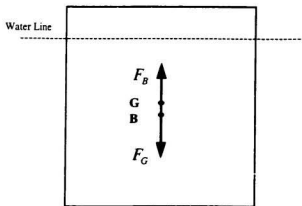


Figure 3-1 Vertical cross-section of an icebrg

Once the equilibrium is broken, such as due to melting, fragmentation or an external force, the iceberg will go to a new stable position. In order to determine the new stable position, a clear understanding of hydrostatic stability is needed.

3.3 Shape definition and coordinate system transformation

3.3.1 Shape definition

A right-handed Cartesian coordinate system is used in this thesis as shown in Figure 3-2). Any change of orientation can be broken up into 3 individual rotations. The standard order is: first yaw, then pitch, and finally roll.

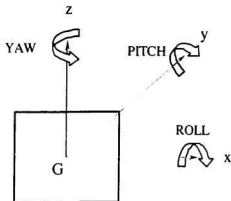


Figure 3-2 Body coordinate system

The choice of method for representing the natural surfaces of icebergs in detail is directed by the need for flexibility to describe the shape, keep track of and update shape changes, determine hydrostatic, floatation, and stability characteristics, and evaluate stresses.

A set of inertial, or space system denoted as $O(x_o, y_o, z_o)$ is fixed with respect to the undisturbed water surface with the z_o axis pointing up. A non-inertia, or body system $I(x_i, y_i, z_i)$ is fixed with respect to the centre of mass of an iceberg. The surface of an iceberg is divided into a series of triangles. Each triangle is defined by three points

(x_i, y_i, z_i) in a body system and a unit normal vector \hat{n} inside the body. Each point in a triangle is explicitly associated with two nearby points to form a triangular surface plane: unit tangents from the surface point to its two associated points define the surface normal (\times product). The set of elemental triangular areas constitute the discretized surface area. The relationship between space coordinate system and body system is shown in Figure 3-3.

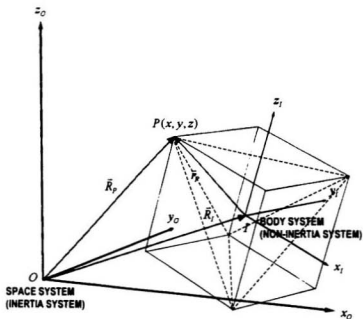


Figure 3-3 Space and body coordinate systems

Changes in shape due to continuous ablation processes are evaluated at each point at specified time intervals; likewise the surface normals are evaluated at each point using the new positions of the surface points. As the ablation processes involve a variety of environmental conditions that are more or less directional, it is necessary that the vectors defined in the body system be known in the space or inertial system as well. This can be done with the appropriate coordinate system transformations (see e.g. Abkowitz 1969).

3.3.2 Coordinate system transformation: position, translation velocity, and force vectors

The orientation of a body axes relative to inertial axes is given by three consecutive rotations through the Eulerian angles (Φ, Θ, Ψ) . The coordinate transformation method used here follows Abkowitz (1969). In Figure 3-4, a body axes system x_1, y_1, z_1 is shown with its initial orientation equal to some fixed axes (which for convenience can be assumed to be coincident with x_1, y_1, z_1). The first rotation is about the z_1 axis through an azimuth angle Ψ ; the rotated body axes become x_2, y_2, z_2 . The rotation matrix $T(\Psi)$ is given in Eqn. (3.1).

$$T(\Psi) = \begin{bmatrix} \cos\Psi & \sin\Psi & 0 \\ -\sin\Psi & \cos\Psi & 0 \\ 0 & 0 & 1 \end{bmatrix} \quad (3.1)$$

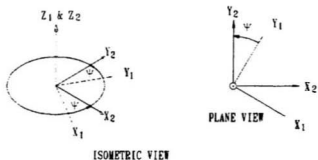


Figure 3-4 Rotation of body axes through azimuth angle Ψ

The second rotation is about the y_2 axis through the trim angle Θ , as illustrated in Figure 3-5. The rotated body axes become x_3 , y_3 , z_3 . Its transformation matrix $T(\Theta)$ is

$$T(\Theta) = \begin{bmatrix} \cos \Theta & 0 & -\sin \Theta \\ 0 & 1 & 0 \\ \sin \Theta & 0 & \cos \Theta \end{bmatrix} \quad (3.2)$$

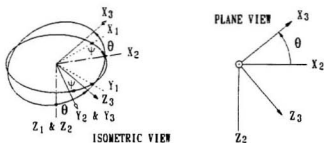


Figure 3-5 Rotation of body axes through trim angle Θ

The third rotation is about the x_3 axis through the roll angle Φ , as shown in Figure 3-6 where the x, y, z axes give the final orientation of the body with respect to the space axes x_o, y_o, z_o . Its rotation matrix is $T(\Phi)$, written as

$$T(\Phi) = \begin{bmatrix} 1 & 0 & 0 \\ 0 & \cos \Phi & \sin \Phi \\ 0 & -\sin \Phi & \cos \Phi \end{bmatrix} \quad (3.3)$$

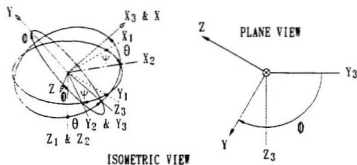


Figure 3-6 Rotation of body axes through roll angle Φ

These three rotations must be done in this order to arrive at the required body axes orientation. The rotation matrices can be combined to give the transformation matrix T_T :

$$\mathbf{T}_T = \mathbf{T}(\Phi)\mathbf{T}(\Theta)\mathbf{T}(\Psi) = \begin{bmatrix} \cos\Theta\cos\Psi & \cos\Theta\sin\Psi & -\sin\Theta \\ \sin\Phi\sin\Theta\cos\Psi - \cos\Phi\sin\Psi & \sin\Phi\sin\Theta\sin\Psi + \cos\Phi\cos\Psi & \sin\Phi\cos\Theta \\ \cos\Phi\sin\Theta\cos\Psi + \sin\Phi\sin\Psi & \cos\Phi\sin\Theta\sin\Psi - \sin\Phi\cos\Psi & \cos\Phi\cos\Theta \end{bmatrix} \quad (3.4)$$

where the subscript T denotes that this transformation is for translational velocity, position, and force vectors. The inverse of this transformation is \mathbf{T}_T^{-1} given by

$$\mathbf{T}_T^{-1} = \begin{bmatrix} \cos\Theta\cos\Psi & \sin\Phi\sin\Theta\cos\Psi - \cos\Phi\sin\Psi & \cos\Phi\sin\Theta\cos\Psi + \sin\Phi\sin\Psi \\ \cos\Theta\sin\Psi & \sin\Phi\sin\Theta\sin\Psi + \cos\Phi\cos\Psi & \cos\Phi\sin\Theta\sin\Psi - \sin\Phi\cos\Psi \\ -\sin\Theta & \sin\Phi\cos\Theta & \cos\Phi\cos\Theta \end{bmatrix} \quad (3.5)$$

To apply the coordinate system transformation and the inverse transformation to the calculation, let us consider the position vector \bar{r}_p , which locates a point $P(x, y, z)$ on a body's surface and whose components are given in its body axes. Given the position vector in space of the body axes' origin, I , by \bar{R}_I , and the orientation angles (Φ, Θ, Ψ) , the position vector in the space axes of the point $P(x, y, z)$ is given by \bar{R}_p (shown in Figure 3-3):

$$\bar{R}_p = \bar{R}_I + \mathbf{T}_T^{-1}\bar{r}_p \quad (3.6)$$

The components of a vector given in the space coordinate system are determined in a body coordinate system oriented at angles (Φ, Θ, Ψ) to the space axes by the

transformation matrix in Eqn. (3.4). The inverse transformation is applied in the opposite case, such as in Eqn. (3.5), when components of a vector given in a body axes system are to be determined in the space axes.

3.3.3 Coordinate system transformation: angular velocity vectors

Excepting position, velocity, and force vectors, angular velocity and angular acceleration are needed to describe the motion of the iceberg. Angular velocities $\dot{\psi}$, $\dot{\theta}$, and $\dot{\phi}$ in space system are applied to the iceberg in succession and the angular velocity ω in body system is determined by summing the vector components of azimuth, trim, and roll velocities. Again the method presented here follows Abkowitz (1969).

Beginning with the azimuth velocity $\dot{\psi}$, the azimuth component of ω is

$$\begin{Bmatrix} p \\ q \\ r \end{Bmatrix}_{\Psi} = \mathbf{T}(\Phi)\mathbf{T}(\Theta)\mathbf{T}(\Psi) \begin{Bmatrix} 0 \\ 0 \\ \dot{\psi} \end{Bmatrix} \quad (3.7)$$

where p , q , and r are the components of the angular velocity vector ω about the body system's x , y , and z axes.

Applying the trim velocity $\dot{\theta}$ second, the trim component of ω is

$$\begin{Bmatrix} p \\ q \\ r \end{Bmatrix}_{\theta} = \mathbf{T}(\Phi)\mathbf{T}(\Theta) \begin{Bmatrix} 0 \\ \dot{\Theta} \\ 0 \end{Bmatrix} \quad (3.8)$$

Ending with the roll velocity $\dot{\Phi}$, the roll component of ω is

$$\begin{Bmatrix} p \\ q \\ r \end{Bmatrix}_{\Phi} = \mathbf{T}(\Phi) \begin{Bmatrix} \dot{\Phi} \\ 0 \\ 0 \end{Bmatrix} \quad (3.9)$$

Thus the total angular velocity, ω , is given by

$$\begin{aligned} \omega = \begin{Bmatrix} p \\ q \\ r \end{Bmatrix} &= \begin{Bmatrix} p \\ q \\ r \end{Bmatrix}_{\Psi} + \begin{Bmatrix} p \\ q \\ r \end{Bmatrix}_{\theta} + \begin{Bmatrix} p \\ q \\ r \end{Bmatrix}_{\Phi} \\ &= \mathbf{T}(\Phi)\mathbf{T}(\Theta)\mathbf{T}(\Psi) \begin{Bmatrix} 0 \\ 0 \\ \dot{\Psi} \end{Bmatrix} + \mathbf{T}(\Phi)\mathbf{T}(\Theta) \begin{Bmatrix} 0 \\ \dot{\Theta} \\ 0 \end{Bmatrix} + \mathbf{T}(\Phi) \begin{Bmatrix} \dot{\Phi} \\ 0 \\ 0 \end{Bmatrix} \end{aligned} \quad (3.10)$$

which reduces to

$$\omega = \begin{Bmatrix} p \\ q \\ r \end{Bmatrix} = \mathbf{T}_R \begin{Bmatrix} \dot{\Phi} \\ \dot{\Theta} \\ \dot{\Psi} \end{Bmatrix} \quad (3.11)$$

where the transformation matrix is

$$\mathbf{T}_R = \begin{bmatrix} 1 & 0 & -\sin \Theta \\ 0 & \cos \Phi & \sin \Phi \cos \Theta \\ 0 & -\sin \Phi & \cos \Phi \cos \Theta \end{bmatrix} \quad (3.12)$$

The inverse transformation matrix can be used to find the angular velocity components $\dot{\Psi}, \dot{\Theta}$, and $\dot{\Phi}$, when p, q , and r are known in the body system. It is written as

$$\mathbf{T}_R^{-1} = \begin{bmatrix} 1 & \sin \Phi \tan \Theta & \cos \Phi \tan \Theta \\ 0 & \cos \Phi & -\sin \Phi \\ 0 & \sin \Phi \sec \Theta & \cos \Phi \sec \Theta \end{bmatrix} \quad (3.13)$$

3.4 Pressure integration technique

Classical methods of calculating hydrostatic stability, either initial stability or dynamic stability, rely on the calculation of centre of buoyancy and metacentre. Then the position of the centre of buoyancy is determined from the submerged volume and the position of the metacentre arises from consideration of the water plane's second moments of area. This approach to hydrostatic stability faces the difficulties of calculating hydrostatic characteristics of an arbitrary shaped body by using its volume and water plane area, and suffers from a very restrictive range of validity, such as the small angle assumption and the 'wall-sided' assumption. In this thesis, another more fundamental

approach is used; the physically more realistic pressure distribution acting over the submerged body surface. The pressure integration technique (Witz & Patel, 1984, Harrison et al. 1989) is used to yield all the hydrostatic characteristics of the ice body. This method is a transformation of surface integrals to volume integrals that allows conventional naval architectural quantities to be derived directly from the integration of surface pressure. The method is implemented in a general purpose program that can compute the hydrostatic characteristics of an arbitrary shaped floating body, with the body surface defined as a series of panels. The pressure integration technique allows complex geometries to be modelled accurately and provides accurate results for large angle rotations. This method requires good discretization. In this thesis, the smooth surface of the iceberg is re-meshed and the entire body surface is divided into panels, such as triangles. This mesh process can be done by some meshing tools or some 3-dimensional model construction tools.

Consider the arbitrary body shown in Figure 3-7 floating at the free surface between air and water. The air is at a constant pressure equal to the free surface pressure. The pressure is assumed to be constant across the free surface. The pressure P of the water with respect to the free surface at any point (x, y, z) in space system below the free surface is:

$$P = \rho_w g z \quad (3.14)$$

where ρ_w is the density of water, and g is the acceleration due to gravity. There are two forces acting on the body. The first force is the weight of the body acting vertically downwards. The second force is due to the fluid pressure acting on the body's submerged surface. The incremental force $d\vec{F}$ acting on the a small surface patch $d\vec{S}$ due to fluid pressure is

$$d\vec{F} = \rho_w g z \cdot d\vec{S} \quad (3.15)$$

$$d\vec{F} = \rho_w g z \cdot \hat{n} dS \quad (3.16)$$

By integrating over the submerged surface of the body, the total buoyancy force, \vec{F}_b , is

$$\vec{F}_b = \rho_w g \iint_S z \cdot \hat{n} dS \quad (3.17)$$

where \hat{n} is the unit normal vector acting into the body and is a function of position vector $\vec{R}(x, y, z)$. Similarly, the incremental roll moment about the centre of gravity, due to buoyancy, $d\vec{M}$ is:

$$d\vec{M} = \vec{R} \times d\vec{F} = \vec{R} \times \rho_w g z \cdot \hat{n} dS \quad (3.18)$$

Integrating

$$\vec{M} = \rho_w g \iiint_V \vec{R} \times \vec{z} \cdot \hat{n} dS \quad (3.19)$$

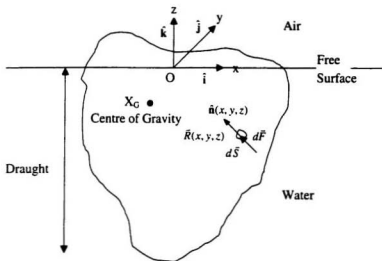


Figure 3-7 Floating body equilibrium

To compute the mass moment of inertia, product of inertia, which are associated with the volume integration, the divergence theorem is used here to transform volume integration to surface integration.

$$\iiint_V \left(\frac{\partial P}{\partial x} + \frac{\partial Q}{\partial y} + \frac{\partial R}{\partial z} \right) dV = \oint_S (P dS_x + Q dS_y + R dS_z) \quad (3.20)$$

where dS_x , dS_y , and dS_z are projections of an element of the surface S in the x , y and z direction respectively pointing outwards from the surface of volume V .

In order to simulate the motion of an iceberg, we need to know its generalized mass matrix, such as the mass of the iceberg, the moment of inertia and the product of inertia, which is described as follows.

3.5 Volume and centre of mass

3.5.1 Volume of the ice model

The model assumes the ice has constant density. An Arctic iceberg can reasonably be assumed to be of constant density (see Gammon et al 1983), although this assumption is not always correct for Antarctic icebergs. In the present case the centroid of the volume is equivalent to the centre of mass.

The total weight of the iceberg at rest in static equilibrium is equal to the buoyancy. In order to obtain the volume of the ice model, let us assume the whole body is submerged into the water, the total buoyancy $F_{B-Total}$ is

$$F_{B-Total} = \rho_w g V \quad (3.21)$$

which is also equal to the total vertical force due to hydrostatic pressure, for a full submerged iceberg.

$$F_{B-Total} = \rho_w g \oint_{S_T} z \cdot \hat{n} dS \quad (3.22)$$

where the subscript S_T means the total surface of the iceberg.

From the Eqn. (3.21) and Eqn. (3.22), the volume of the submerged body V , where based on our assumption the volume of the ice model, can be calculated by

$$V = \oint_{S_T} z \cdot \hat{n} dS \quad (3.23)$$

3.5.2 Weight of the ice model

Because the body is in equilibrium, the weight F_G is equal to the buoyancy F_B

$$F_G = F_B = \rho_w g \oint_{S_T} z \cdot \hat{n} dS \quad (3.24)$$

where S_s is submerged surface of the ice model.

3.5.3 Centre of the buoyancy and centre of the mass

By applying the pressure integration technique and the divergence theorem, and integrating over the whole submerged surface, S_s , of the body, we can write the centre of buoyancy as follows:

$$x_B = \frac{\iint_{S_s} zx \cdot \hat{n} dS}{\iint_{S_s} z \cdot \hat{n} dS} \quad (3.25)$$

$$y_B = \frac{\iint_{S_s} zy \cdot \hat{n} dS}{\iint_{S_s} z \cdot \hat{n} dS} \quad (3.26)$$

$$z_B = \frac{\iint_{S_s} \frac{z^2}{2} \cdot \hat{n} dS}{\iint_{S_s} z \cdot \hat{n} dS} \quad (3.27)$$

through integrating the total surface, S_T , of the body, the centre of the mass can be yielded

$$x_G = \frac{\iint_{S_f} zx \cdot \hat{n} dS}{\iint_{S_f} z \cdot \hat{n} dS} \quad (3.28)$$

$$y_G = \frac{\iint_{S_f} zy \cdot \hat{n} dS}{\iint_{S_f} z \cdot \hat{n} dS} \quad (3.29)$$

$$z_G = \frac{\iint_{S_f} \frac{z^2}{2} \cdot \hat{n} dS}{\iint_{S_f} z \cdot \hat{n} dS} \quad (3.30)$$

3.6 Water plane area

The water plane area S_w can also be derived from the pressure integration technique as

$$S_w = \iint_{S_f} \hat{k} \cdot \hat{n} dS \quad (3.31)$$

where \hat{k} is unit vector in z direction in space system (shown in Figure 3-7), and \hat{i}, \hat{j} are unit vectors in x and y direction, respectively.

3.7 Properties of ice body

In order to simulate the motion of the iceberg, we need know the other mass properties, such as moments of inertia and products of inertia. All of these elements can be obtained through volume integration. Here we use the divergence theorem to transform volume integration to surface integration.

3.7.1 Moment of inertia and product of inertia

The method used in this thesis to transfer volume integration to surface integration is described as follows. The transformation is based on the divergence theorem (see Eqn. (3.20)).

$$\begin{aligned} I_{xx} &= \rho_i \iiint_V (y^2 + z^2) dV \\ &= \rho_i \oint_S [(\frac{2}{3} y^3 + yz^2 - y^2 z) dS_x + (\frac{2}{3} y^3 + yz^2 - y^2 z) dS_y + (\frac{2}{3} y^3 + yz^2 - y^2 z) dS_z] \end{aligned} \quad (3.32)$$

$$\begin{aligned} I_{yy} &= \rho_i \iiint_V (x^2 + z^2) dV \\ &= \rho_i \oint_S [(\frac{2}{3} x^3 + xz^2 - x^2 z) dS_x + (\frac{2}{3} x^3 + xz^2 - x^2 z) dS_y + (\frac{2}{3} x^3 + xz^2 - x^2 z) dS_z] \end{aligned} \quad (3.33)$$

$$\begin{aligned}
I_x &= \rho_i \iiint_V (x^2 + y^2) dV \\
&= \rho_i \oint\oint_S [(\frac{2}{3}x^3 + xy^2 - x^2y)dS_x + (\frac{2}{3}x^3 + xy^2 - x^2y)dS_y + (\frac{2}{3}x^3 + xy^2 - x^2y)dS_z] \quad (3.34)
\end{aligned}$$

$$\begin{aligned}
I_y &= \rho_i \iiint_V xy dV \\
&= \rho_i \oint\oint_S [(-\frac{1}{6}x^3 + \frac{1}{2}x^2y)dS_x + (-\frac{1}{6}x^3 + \frac{1}{2}x^2y)dS_y + (-\frac{1}{6}x^3 + \frac{1}{2}x^2y)dS_z] \quad (3.35)
\end{aligned}$$

$$\begin{aligned}
I_z &= \rho_i \iiint_V xz dV \\
&= \rho_i \oint\oint_S [(-\frac{1}{6}x^3 + \frac{1}{2}x^2z)dS_x + (-\frac{1}{6}x^3 + \frac{1}{2}x^2z)dS_y + (-\frac{1}{6}x^3 + \frac{1}{2}x^2z)dS_z] \quad (3.36)
\end{aligned}$$

$$\begin{aligned}
I_{yz} &= \rho_i \iiint_V yz dV \\
&= \rho_i \oint\oint_S [(-\frac{1}{6}y^3 + \frac{1}{2}y^2z)dS_x + (-\frac{1}{6}y^3 + \frac{1}{2}y^2z)dS_y + (-\frac{1}{6}y^3 + \frac{1}{2}y^2z)dS_z] \quad (3.37)
\end{aligned}$$

3.8 Coordinate system transformation in simulation

3.8.1 Initial transformation matrix

The construction of the coordinate system transformation matrix has been described above in section 3.3. Here we use \mathbf{T}_0 as the initial transformation matrix, and \mathbf{T}_0^{-1} as the initial inverse transformation matrix.

3.8.2 Simulation process

Assuming at time t_1 that the ice model has rotated through three small angles ψ_1, θ_1, ϕ_1 compared with its initial status, and then the transformation matrix from space system to body system is denoted as:

$$\mathbf{T} = \mathbf{T}_1 \mathbf{T}_0 \quad (3.38)$$

and the transformation matrix from body system to space system is denoted as:

$$\mathbf{T}^{-1} = \mathbf{T}_0^{-1} \mathbf{T}_1^{-1} \quad (3.39)$$

At time t_n , the corresponding transformation matrices become:

$$\mathbf{T} = \mathbf{T}_n \mathbf{T}_{n-1} \cdots \mathbf{T}_1 \mathbf{T}_0 \quad (3.40)$$

$$\mathbf{T}^{-1} = \mathbf{T}_0^{-1} \mathbf{T}_1^{-1} \cdots \mathbf{T}_{n-1}^{-1} \mathbf{T}_n^{-1} \quad (3.41)$$

3.9 Equations of motion for a body moving with six degrees

3.9.1 Motion equations

It is assumed that the motions of the iceberg are linear and harmonic. An iceberg floating at sea is allowed to move in all the six degrees of freedom of motion, i.e. translation along three orthogonal axes and rotation about each of the three axes. So it is necessary to choose an axis system to describe these motions and the choice should be one that is most convenient for the development of the motion analysis. To this end, a right-handed coordinate system (x, y, z) fixed with respect to the mass centre of the ice model with z vertically upward is used, which has been described in section 3.3. The translatory displacements in the x , y , and z directions with respect to the origin are η_1 , η_2 , and η_3 , respectively, so that η_1 is the surge, η_2 is the sway, and η_3 is the heave displacement. The angular displacements due the rotational motion about the x , y , and z axes are η_4 , η_5 , and η_6 , respectively, where η_4 is the roll, η_5 is the pitch, and η_6 is the yaw angle (Salvesen, Tuck and Faltinsen, 1970).

Under the assumptions that the responses are linear and harmonic, the six linear coupled differential equations of motion, without exciting force and moment, can be written as:

$$\sum_{k=1}^6 [(M_{jk} + A_{jk})\ddot{\eta}_k + B_{jk}\dot{\eta}_k + C_{jk}\eta_k] = 0; j = 1 \dots 6 \quad (3.42)$$

where M_{jk} are the components of the generalized mass matrix for the ice mass, A_{jk} and B_{jk} are the added-mass and damping coefficients, and C_{jk} are the hydrostatic restoring coefficients. The weight, buoyancy, and the moments (i.e. all the C_{jk} terms) due to the difference between the weight and the buoyancy are taken in the thesis, as the external forces that govern the motion of the model.

During the simulation processes, the generalized mass matrix of the iceberg, the position and the orientation of the iceberg will be updated continuously. Considering at some time t_n , which is a time interval Δt past the time t_{n-1} , the iceberg moves and rotates a very small displacement and angle compared with the position and the orientation at the time t_{n-1} . This is the reason small angle theory is adopted in this thesis.

In the model, the added mass coefficients and damping coefficients are taken to be constants during the whole simulation process. In reality, all of these coefficients are related to the iceberg's shape and frequency of oscillation. Improvement of the added mass and damping coefficients are recommended for later version of this model.

The Runge-Kutta method (Pachner, 1984) was used to solve the motion equations.

In order to simplify the problem, some other couplings between hydrodynamical effects are neglected. So the other nondiagonal elements in added-mass and damping

matrices are eliminated. This might be a good first approximation for the iceberg stability analysis.

The equations in matrix style can be rewritten as;

$$\begin{pmatrix} M & & & & & \\ & M & & & & \\ & & M & & & \\ & & & I_{xx} & -I_{xy} & -I_{xz} \\ & & & -I_{xy} & I_{yy} & -I_{yz} \\ & & & -I_{xz} & -I_{yz} & I_{zz} \end{pmatrix} + \begin{pmatrix} A_{11} & & & & & \\ & A_{22} & & & & \\ & & A_{33} & & & \\ & & & A_{44} & & \\ & & & & A_{55} & \\ & & & & & A_{66} \end{pmatrix} \begin{pmatrix} \ddot{x} \\ \ddot{y} \\ \ddot{z} \\ \ddot{\phi} \\ \ddot{\theta} \\ \ddot{\psi} \end{pmatrix} + \begin{pmatrix} B_{11} & & & & & \\ & B_{22} & & & & \\ & & B_{33} & & & \\ & & & B_{44} & & \\ & & & & B_{55} & \\ & & & & & B_{66} \end{pmatrix} \begin{pmatrix} \dot{x} \\ \dot{y} \\ \dot{z} \\ \dot{\phi} \\ \dot{\theta} \\ \dot{\psi} \end{pmatrix} = \begin{Bmatrix} \{Force\} \\ \{Moment\} \end{Bmatrix} \quad (3.43)$$

In compact model

$$\mathbf{M} \begin{Bmatrix} \ddot{x} \\ \ddot{y} \\ \ddot{z} \\ \ddot{\phi} \\ \ddot{\theta} \\ \ddot{\psi} \end{Bmatrix} + \mathbf{B} \begin{Bmatrix} \dot{x} \\ \dot{y} \\ \dot{z} \\ \dot{\phi} \\ \dot{\theta} \\ \dot{\psi} \end{Bmatrix} = \begin{Bmatrix} \{Force\} \\ \{Moment\} \end{Bmatrix} \quad (3.44)$$

where \mathbf{M} is generalized mass matrix. Detaching the variables

$$\mathbf{M}^{-1}\mathbf{M}\begin{Bmatrix} \ddot{x} \\ \ddot{y} \\ \ddot{z} \\ \ddot{\phi} \\ \ddot{\theta} \\ \ddot{\psi} \end{Bmatrix} + \mathbf{M}^{-1}\mathbf{B}\begin{Bmatrix} \dot{x} \\ \dot{y} \\ \dot{z} \\ \dot{\phi} \\ \dot{\theta} \\ \dot{\psi} \end{Bmatrix} = \mathbf{M}^{-1}\begin{Bmatrix} \{Force\} \\ \{Moment\} \end{Bmatrix} \quad (3.45)$$

$$\begin{Bmatrix} \ddot{x} \\ \ddot{y} \\ \ddot{z} \\ \ddot{\phi} \\ \ddot{\theta} \\ \ddot{\psi} \end{Bmatrix} = \mathbf{M}^{-1}\begin{Bmatrix} \{Force\} \\ \{Moment\} \end{Bmatrix} - \mathbf{M}^{-1}\mathbf{B}\begin{Bmatrix} \dot{x} \\ \dot{y} \\ \dot{z} \\ \dot{\phi} \\ \dot{\theta} \\ \dot{\psi} \end{Bmatrix} \quad (3.46)$$

$$\frac{d^2\eta_i(t)}{dt^2} = f_i(x, y, z, \phi, \theta, \psi, \dot{x}, \dot{y}, \dot{z}, \dot{\phi}, \dot{\theta}, \dot{\psi}); i = 1 \dots 6 \quad (3.47)$$

If define $F(x, y, z, \phi, \theta, \psi) = \text{Buoyancy} - \text{Weight}$, then

$$\frac{d^2\eta_i(t)}{dt^2} = f_i[F(x, y, z, \phi, \theta, \psi), \dot{x}, \dot{y}, \dot{z}, \dot{\phi}, \dot{\theta}, \dot{\psi}]; i = 1 \dots 6 \quad (3.48)$$

3.9.2 Forces and moments

3.9.2.1 Buoyancy and buoyancy centre

The buoyancy and buoyancy centre can be calculated from equation (3.22), (3.25), (3.26) and (3.27).

3.9.2.2 Moment in space system

The moment acting on the ice model in space system in x direction and y direction can be written as

$$M_x = F_B(y_B - y_w) \quad (3.49)$$

and

$$M_y = -F_B(x_B - x_w) \quad (3.50)$$

3.9.2.3 Force and moment in body system

By applying the transformation matrix, the force and moment acting on the ice model can be converted from space system to body system by

$$\{Force\} = \begin{Bmatrix} F_1 \\ F_2 \\ F_3 \end{Bmatrix} = T \begin{Bmatrix} 0 \\ 0 \\ F_B - F_G \end{Bmatrix} \quad (3.51)$$

and

$$\{Moment\} = \begin{Bmatrix} M_4 \\ M_5 \\ M_6 \end{Bmatrix} = T \begin{Bmatrix} M_x \\ M_y \\ 0 \end{Bmatrix} \quad (3.52)$$

3.10 Coefficient selection

Hydrodynamic coefficients such as added mass and damping are important in the simulation model. In this thesis, in order to simplify our model, we regard the added mass coefficients and damping coefficients as constants during the whole simulation process. The selection of all of these coefficients depends on the iceberg shape and frequency of oscillation, and the mass and the length of the iceberg are used for non-dimensionalisation (Shown in Table 3-1). Bass and Sen's (1986) coefficients were used as a reference here. The exact coefficients need to be calibrated using the experimental data in the future.

Table 3-1 Normalizing factors (Bass & Sen, 1986)

Parameter		Dimensionless	Dimensionless
Description	Symbol	(Factor)	(Parameter)

Surge added mass coeff.	A_{11}	m	$[A_{11}] = A_{11} / m$
Sway added mass coeff.	A_{22}	m	$[A_{22}] = A_{22} / m$
Heave added mass coeff.	A_{33}	m	$[A_{33}] = A_{33} / m$
Roll added moment coeff.	A_{44}	mL^2	$[A_{44}] = A_{44} / (mL^2)$
Pitch added moment coeff.	A_{55}	mL^2	$[A_{55}] = A_{55} / (mL^2)$
Yaw added moment coeff.	A_{66}	mL^2	$[A_{66}] = A_{66} / (mL^2)$
Surge damping coeff.	B_{11}	$m\sqrt{(g/L)}$	$[B_{11}] = B_{11} / (m\sqrt{(g/L)})$
Sway damping coeff.	B_{22}	$m\sqrt{(g/L)}$	$[B_{22}] = B_{22} / (m\sqrt{(g/L)})$
Heave damping coeff.	B_{33}	$m\sqrt{(g/L)}$	$[B_{33}] = B_{33} / (m\sqrt{(g/L)})$
Roll damping coeff.	B_{44}	$mL^2\sqrt{(g/L)}$	$[B_{44}] = B_{44} / (mL^2\sqrt{(g/L)})$
Pitch damping coeff.	B_{55}	$mL^2\sqrt{(g/L)}$	$[B_{55}] = B_{55} / (mL^2\sqrt{(g/L)})$
Yaw damping coeff.	B_{66}	$mL^2\sqrt{(g/L)}$	$[B_{66}] = B_{66} / (mL^2\sqrt{(g/L)})$

m =mass; L =berg length; g =gravitational acceleration

3.11 Simulation method

The Runge-Kutta method is used to solve the motion equation (3.48). Details of the Runge-Kutta method are described in Appendix A.

3.12 Potential energy map

A potential energy method is used to determine the equilibrium positions that an arbitrarily shaped body can assume. The energy approach is used here because it lends

itself to a thorough evaluation of the iceberg's possible stable orientations. This is useful information because of the large number of possible stable orientations (Bass & Peters 1984, Lever et al. 1991).

For a given orientation, the draft at which the static equilibrium ($F_G = F_B$) is satisfied can be found by iteration. The iteration routine finds the position at which the ratio of underwater volume to total volume is equal to the ratio of iceberg density to water density. Alternatively, it can be found directly by integrating the pressure on the underwater surface until the buoyancy is equal to the known weight. For each orientation (pitch/roll combination) the potential energy is found from the vertical distance between the centres of gravity and buoyancy, \overline{BG} . Stable equilibrium positions occur at minima of the energy function.

$$E(\Theta, \Phi) = \rho_w g V \overline{BG} \quad (3.53)$$

3.13 Computer program design

A computer program named STABLE has been developed to simulate the dynamic stability process, the stability changes due to melting, and the motion changes of the iceberg due to some external forces. The interface of STABLE is shown in Figure 3-8. The program is developed using Microsoft Visual C++ language and OpenGL graphics library. The program has five modules. They are: static analysis of floating position and

orientation; dynamic stability simulation; potential energy calculation; melting simulation, and, towing and drag force simulation.

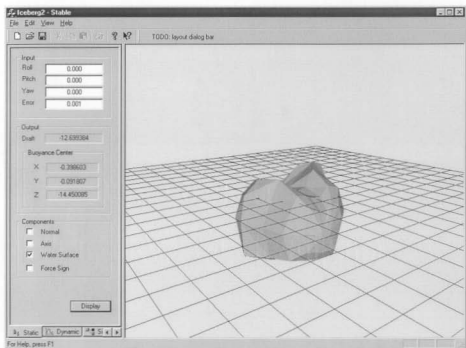


Figure 3-8 User Interface of the STABLE program.

Here two key points of the program design are described. One is the input file format, and the other is the data structure of the model in the program.

3.13.1 Format of input file

The Stereolithography, or STL file format is used to input the iceberg model into the program. The Stereolithography format is an industry standard that is used to store 3-dimensional models in many CAD software or finite element software. There are two reasons to choose this file format. One is that the STL file format can store 3-dimensional model information in a text format. It is easy to view and modify. The other is that we can use many widely used engineering software packages, such as AutoCAD and Rhino to mesh and construct an iceberg model.

A sample STL file, a box (10m×10m×10m) model, is listed in Appendix C as a reference.

3.13.2 Data structure of the model in the program

To make the program work efficiently, a special data structure is designed to describe the model in the program (shown in Figure 3-9). More details of the program design are presented in Appendix A.

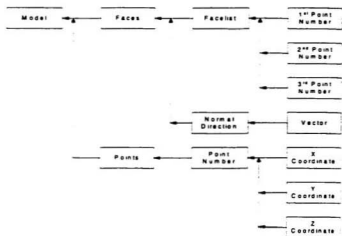


Figure 3-9 Data structure of the model in program

Chapter 4

Results and Discussion

The results of the numerical model and program, described in Chapter 3, are discussed in this Chapter. The initial aim of this research is to construct the relationship between the shape changes and stability of the iceberg. For a complex ice model, the shape changes due to the melting are hard to describe or re-mesh, and some adaptive mesh geometry technology needs to be employed. Adaptive meshing is outside the scope of this thesis. For this reason, some simple ice shapes are adopted to demonstrate the melting process. On the other hand, because the correlation of the stability and motion is well constructed and programmed, more attention will be paid to the model motion simulation.

In this Chapter, the iceberg deterioration and stability model will be applied to some icebergs, and then extended to other ocean engineering applications to illustrate its utility. Here five applications are discussed. They are:

- To obtain the most stable position using potential energy map.

- To evaluate and simulate the stability of icebergs.
- To explore the change of stability of an iceberg due to melting.
- To simulate the iceberg towing process.
- To extend to a simple iceberg drift model.

4.1 Potential energy shapes map and motion simulation

Potential energy maps are given for two samples: a relatively small cone ($\varnothing 12\text{m} \times 20\text{m}$ high) and a blocky iceberg (roughly $48\text{m} \times 42\text{m} \times 45\text{m}$). The static potential energy map of a cone is shown in Figure 4-2. A close-up view is shown in Figure 4-3. The solid bold line is the potential energy of the cone during the whole stability simulation process. From these pictures, we can see that the model moves from an unstable position to a stable one. The corresponding dynamic simulation of the cone is shown in Figure 4-1. A similar series of figures for the iceberg shape are shown in Figure 4-5, Figure 4-6 and Figure 4-4. In both cases, we can easily figure out the most stable position, and the maps indicate several local stable positions.

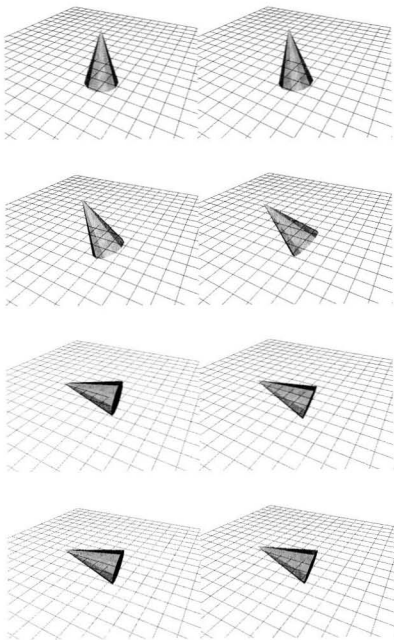


Figure 4-1 Stability simulation of a cone

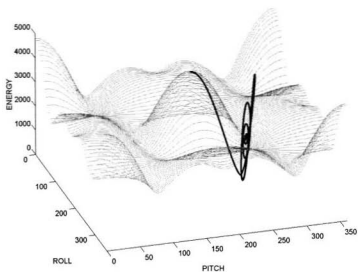


Figure 4-2 Energy map of a cone

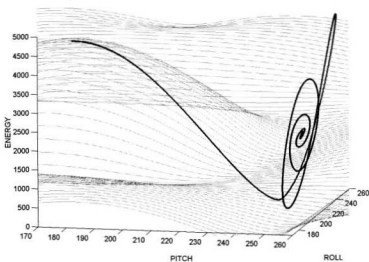


Figure 4-3 Energy map (close) of a cone

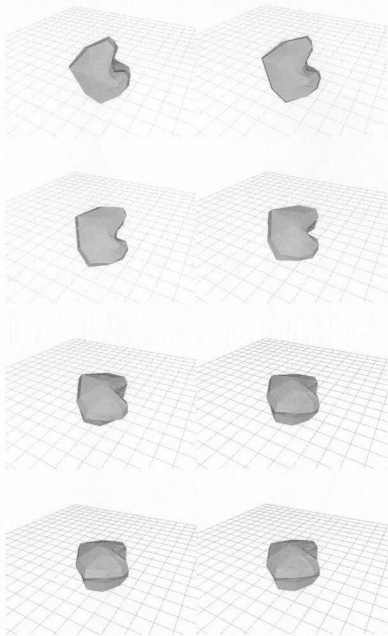


Figure 4-4 Stability simulation of an iceberg

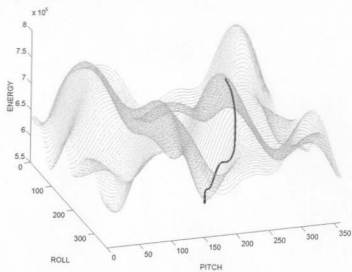


Figure 4-5 Energy map of an iceberg

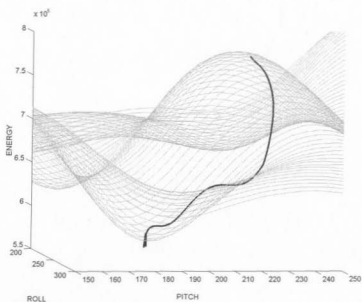


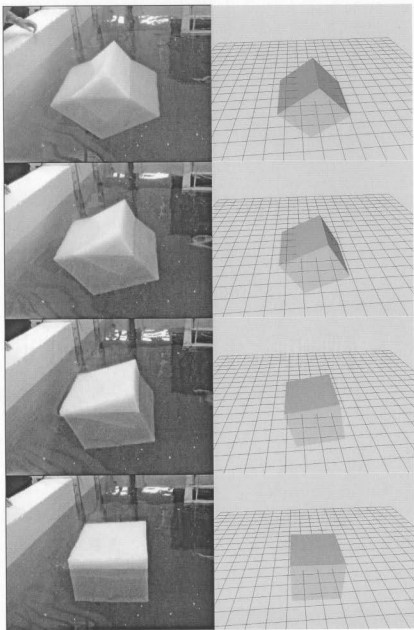
Figure 4-6 Energy map (close) of an iceberg

4.2 Stability evaluation and simulation

The advantage of the pressure integration technique is that it allows complex geometries to be modelled accurately and provides accurate results for large angle rotations. Because the program developed in this thesis integrates the pressure integration technique completely, it is easily to extend to handle some complex models and large angle problems. An example is presented here to illustrate the operation and performance of this pressure integration approach to hydrostatic stability.

A simple test was done in the Fluid and Hydraulics lab in the Memorial University of Newfoundland. A wax cubic model ($0.59\text{m} \times 0.55\text{m} \times 0.48\text{m}$) whose density was the same as the real ice was adopted here. In the test, the cubic ice model was released with some angle in the tank. The movement process was recorded using a digital camera. Similar to the real test, a same dimensional numerical model was input into the program, and released with the same angle. After selecting coefficients carefully, such as added mass coefficient and damping coefficient, the movement process was simulated. The test pictures and simulation pictures were shown in Figure 4-7.

From this example, we can clearly find that the simulation matches the real test very well. The visual simulation of this process will help people to evaluate the stability more accurately.



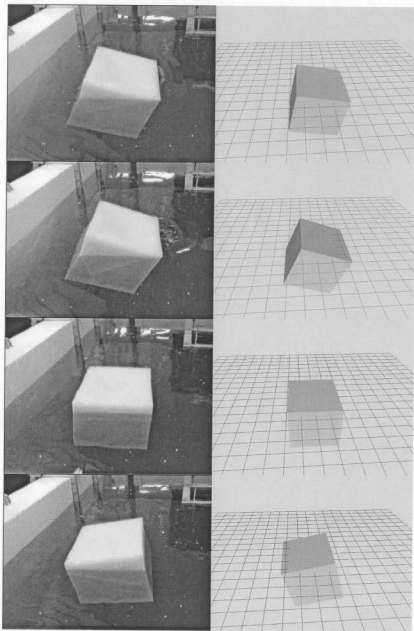


Figure 4-7 Real movement of an ice model compared with the simulation

4.3 Melting simulation

A simulation that incorporates melting and motions for a simple cubic ice model was examined (see Figure 4-8). As the melting proceeds, the block loses stability and rolls. During melting all the mass and geometric properties need to be updated. These properties include the volume, mass, buoyancy centre, weight centre, moments of inertia, and products of inertia. With these changes, the stable positions change. Combining motion and melting does not, in itself, present any difficulties. The mass properties and equations of motion are easy to specify and solve.

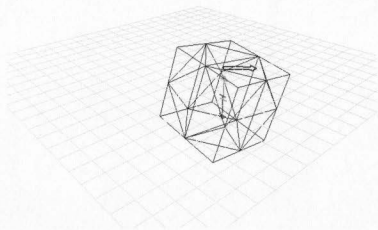
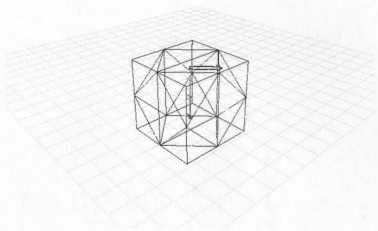


Figure 4-10 Towing force acts above the centre of gravity

4.4 Towing simulation

As a possible application of the STABLE program in iceberg management, a simple towing module is developed. When towing a large iceberg, the initial shape of the iceberg is quite important. If the iceberg is tabular the problems associated with rolling and tipping during the tow should not become significant until the iceberg has been extensively modified by melting and calving (Weeks et al., 1977). If the iceberg is too narrow, or in some marginally stable position, it will be in great danger of rolling over. The minimum requirement is that the metacentric height should be positive, but it would be more reasonable to require a metacentric height at least equal to 10% of the iceberg width. Although the 'classical approach' is easy to compute, it suffers from a very restrictive range of validity, such as small angle assumptions and/or simple geometries. In this program, these restrictions are avoided. Furthermore, the program can simulate towing the iceberg in different positions with different forces.

In order to simplify the problem, we assume that the towing force remains horizontal and acts on the point under or above the centre of gravity (shown in Figure 4-9).

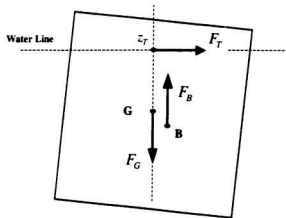


Figure 4-9 Towing force F_T acted on the body at the water surface

Considering the towing force, the overturning moment, \bar{M}_T , can be written as:

$$\bar{M}_T = \bar{F}_T \times (z_T - z_G) \quad (4.1)$$

where \bar{F}_T is the towing force vector and $(z_T - z_G)$ is the vertical distance between the point towing force and the centre of gravity. Comparing with the Eqns. (3.51) and (3.52), the moment and force on the ice become:

$$\{Force\} = \begin{Bmatrix} F_1 \\ F_2 \\ F_3 \end{Bmatrix} = \mathbf{T} \begin{Bmatrix} F_{r_i} \\ F_{r_i} \\ B-W \end{Bmatrix} \quad (4.2)$$

$$\{Moment\} = \begin{Bmatrix} M_4 \\ M_5 \\ M_6 \end{Bmatrix} = \mathbf{T} \begin{Bmatrix} M_x + M_{T_x} \\ M_y + M_{T_y} \\ 0 \end{Bmatrix} \quad (4.3)$$

where F_x , F_y and M_x , M_y are the force and moment in the space system in x and y directions respectively.

A cubic ice model (10m×10m×10m) is used as an example to present the towing process. In the first case, a towing force of 200N, compared with its weight of 8820N, acts at the water surface. It is clear that the ice model tilts downward (see Figure 4-10).

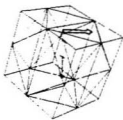
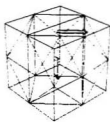


Figure 4-10 Towing force acts above the centre of gravity

In the second case, a towing force of 200N, acts at -6m below the water surface (shown Figure 4-11). The ice model tilts upward compared with the first case (see Figure 4-12).

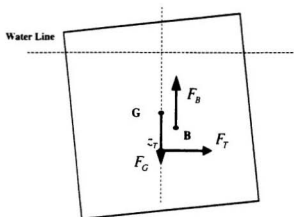


Figure 4-11 Towing force F_T acted on the body below the water surface

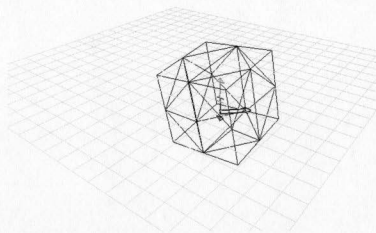
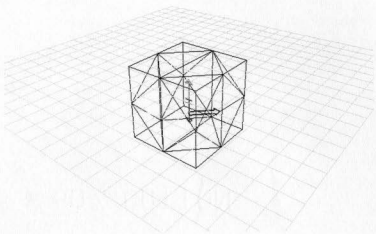
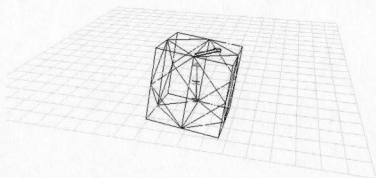
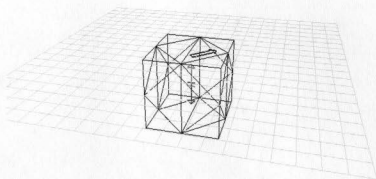


Figure 4-12 Towing force acts under the centre of gravity

When the towing force becomes big enough, in this example 600N, the ice model will roll over during the towing process (see Figure 4-13).



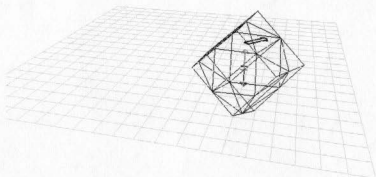
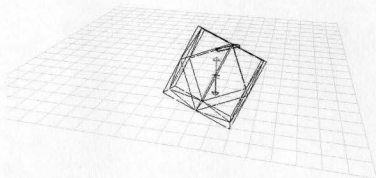


Figure 4-13 Ice model rolls over

4.5 Drift simulation

Another possible application of the programme STABLE in iceberg management is to predict the drift of the iceberg. Because the original aim of this research is to construct the relationship between the shape and the stability of the iceberg, further work needs to be done to forecast the drift of the iceberg. To start, a general review of the iceberg drift mechanism is presented.

An iceberg is assumed to drift under the influence of the vector sum of air drag \vec{F}_A , water drag \vec{F}_D , pressure gradient force \vec{F}_p , radiation force \vec{F}_R of surface waves, Coriolis forcing, and towing force \vec{F}_T (Mountain, D. G., 1980, Smith, S. D. et al., 1983).

$$M(\vec{a} + f \times \vec{V}_i) = \vec{F}_A + \vec{F}_D + \vec{F}_p + \vec{F}_R + \vec{F}_T \quad (4.4)$$

where M , a and V_i are the mass, acceleration and velocity of the iceberg. The Coriolis vector $f = 2\Omega \sin \phi$ points upward; the earth's rate of rotation is $\Omega = 7.272 \times 10^{-5} \text{ rad/s}$ and ϕ is the latitude.

In this thesis, to explore the issue, the problem is simplified, and only considers the water drag force F_D and towing force F_T . The water drag force F_D can be written as

$$F_D = \frac{1}{2} \rho_w D_w A_w |V_w - V_i| \cdot (V_w - V_i) \quad (4.5)$$

where ρ_w is the water density, D_w is the drag coefficient in water, A_w is the submerged cross sectional area in a vertical plane of the iceberg, V_w is the water velocity, and V_i is the iceberg velocity. We assume that the water drag force acts on the buoyancy centre of the iceberg (shown in Figure 4-14). The drag coefficient can be selected from Table 4-1.

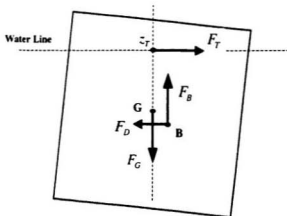





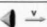



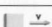


Figure 4-14 Water drag force acted on the body

Table 4-1 Drag coefficients of various 3-D geometrical shapes (from Hoerner, 1965)

SHAPE **	DESCRIPTION	Drag Coefficient D_w
	Solid sphere	0.47
	Half sphere shell	0.38
	Solid half sphere	0.42
	Solid ellipse	0.59
	Solid cube	0.80
	Solid cone	0.50
	Solid half sphere	1.17
	Half sphere shell	1.42
	Half ellipse shell	1.38
	Solid cube	1.05

** V is the flow direction

Considering the water drag force, the moment in x , y , and z direction, M_{D_x} , M_{D_y} , and M_{D_z} separately, can be written as:

$$M_{D_z} = F_{D_z} (z_B - z_G) \quad (4.6)$$

$$M_{D_x} = F_{D_x} (z_B - z_G) \quad (4.7)$$

$$M_{D_z} = F_{D_z} (y_B - y_G) + F_{D_x} (x_B - x_G) \quad (4.8)$$

where F_{D_x} , F_{D_y} , and F_{D_z} is the water drag force in space system in x , y , and z direction.

Integrating the towing force and water drag force, the moment and force on the ice become:

$$\{Force\} = \begin{Bmatrix} F_1 \\ F_2 \\ F_3 \end{Bmatrix} = T \begin{Bmatrix} F_{T_x} + F_{D_x} \\ F_{T_y} + F_{D_y} \\ B - W \end{Bmatrix} \quad (4.9)$$

$$\{Moment\} = \begin{Bmatrix} M_x \\ M_y \\ M_z \end{Bmatrix} = T \begin{Bmatrix} M_x + M_{T_x} + M_{D_x} \\ M_y + M_{T_y} + M_{D_y} \\ M_{D_z} \end{Bmatrix} \quad (4.10)$$

Compared with the towing simulation, the water drag force will affect the tilt angle and velocity of the iceberg motion (in Figure 4-15). For iceberg towing, it is interesting to know how long it will take to accelerate an iceberg up to its full towing speed. Using this model, after considering the other external forces, we can get an accurate result.

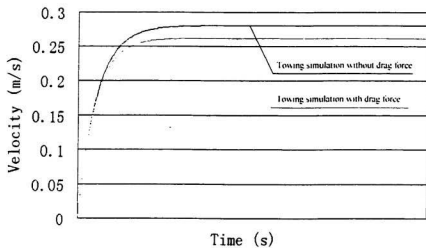


Figure 4-15 Velocities of the iceberg in two situations

Chapter 5

Conclusions and Suggestions for Further Research

Based on the theoretical analysis and simulation presented in this thesis, some conclusions are drawn in this Chapter and suggestions for further research are listed.

5.1 Conclusions

The iceberg deterioration and stability model has been successfully demonstrated to simulate the iceberg motion due to the melting and external forces, such as towing force and water drag force. The simulation process is satisfactory. During this visual simulation process, it can offer valuable information for iceberg management, and be a tool to aid iceberg risk assessment.

A computer program has been developed to model the floatation and stability of an arbitrarily shaped three-dimensional homogeneous floating rigid body, such as an iceberg. Iceberg motions are incorporated into the model and shape changes due to simple melting

are accounted for. As an extension, the towing force and water drag force are also considered.

Using the program, the visual simulation demonstrates the dynamic stability process. The melting/stability model will be used to explore the reasons for the various shapes that icebergs have. To fully explain shape evolution it will be necessary to include calving and fracture, which is beyond the scope of the present model.

5.2 Suggestions for further research

This thesis provides a brief analysis, simulation, applications and some potential applications in the iceberg deterioration and stability study. In order to make this research more applied, much detailed study is needed. The suggestions for further research are outlined as follows:

- The melting section needs to be strengthened. The most problematic aspect of the work is related to describing the evolving shape through an adaptive mesh. The melting model causes awkward results when applied to a general mesh. Some computer graphics technology, such as graphic simplification algorithm, adaptive meshing, can be used to make this work possible.
- Similar to the water drag force, air drag force, pressure gradient force and Coriolis forcing can be added into the program easily.

- More effort should be put on the wave situation, if this program can be used as a practical tool. Considering the wave acting on the iceberg, two effects should be studied respectively. One is the radiation force of surface waves. The other one is iceberg dynamics in waves.

References

- [1] Abkowitz, Martin A. 1969. Stability and motion control of ocean vehicles, The MIT Press, Cambridge, 253 pages. (Appendix II, Notes on Axis Transformations, II-1 – II-8).
- [2] Anon. 1999. Compilation of iceberg shape and geometry data for the Grand Band Banks region. Canatec Consultants Ltd. and others for PERD/CHC Report 20-43, 37 pages + appendices.
- [3] Anon. 1970. WMO sea ice nomenclature. World Meteorological Organisation, No.259.TP.145, Geneva.
- [4] Barker, A., Skabova, I., and Timco, G. 1999. Iceberg visualization database. CHC Report HYD-TR-042, 15 pp.
- [5] Bass, D. W., and Peters, G. R. 1984. Computer simulation of iceberg instability. Cold Regions Science and Technology, Vol.9, pp.163-169.
- [6] Bass, D. W. 1980. Stability of icebergs. Annals of Glaciology, Vol.1, pp.43-47.
- [7] Bass, D. W. and Sen, D. 1986. Added mass and damping coefficient for certain 'realistic' iceberg models. Cold Regions Science and Technology, Vol. 12, pp. 163-174.
- [8] Benedict, C. P. 1980. Dimensional modelling of icebergs. Cold Regions Science and Technology, Vol. 1, No. 3 and 4, pp. 299-306.
- [9] Bigg, G. R., Wadley, M. R., Stevens, D. P., and Johnson, J. A. 1997. Modelling the dynamics and thermodynamics of icebergs. Cold Regions Science and Technology, Vol.26, pp.113-135.

- [10] Budyko, M. I. 1972. The future climate. Trans. Amer. Geophys. Union, Vol.52, pp.868-874.
- [11] Diemand, D. and Lever, J. H. 1986. Iceberg Stress State. Iceberg Research, April 1986, No. 12.
- [12] El-Tahan, M., Venkatesh, S. and EL-Tahan, H. 1984. Validation and Quantitative Assessment of the Deterioration Mechanisms of Arctic Icebergs, Journal of Offshore Mechanics and Arctic Engineering, Vol. 109, pp. 102-108.
- [13] Foren, P. 1969. The waters of the sea. Van Nostrand Reinhold Co., London.
- [14] Gammon, P. H., Gagnon, R. E., Bobby, W., and Russell, W. E. 1983. Physical and mechanical properties of icebergs. Proceedings Offshore Technology Conference, pp. 143-150.
- [15] Griffin, O. M. 1977. Heat, mass, and momentum transfer effects on the ablation of iceberg in seawater. Proceeding Iceberg Utilization, A.A.Husseiny (ed.), Pergamon Press, pp.229-244
- [16] Josberger, E. G. 1977. A laboratory and field study of iceberg deterioration. Proceeding Iceberg Utilization, A.A.Husseiny (ed.), Pergamon Press, pp.245-264
- [17] Hanson, W. E. 1988. Operational iceberg forecasting concerns. Proceedings, Oceans, Vol.2, pp. 561-566.
- [18] Harrison, J. H., Patel, M. H. and Witz, J. A. 1989. Hydrostatic analysis of Naval hull forms using pressure integration. The Royal Institution of Naval Architects.
- [19] Hobbs, P. V. 1974. Ice Physics. Clarndon Press, Oxford.
- [20] Jong, B. De 1973. Net radiation received by a horizontal surface at the earth. Delft Univ. Press, distributed by Academic Book Services, Groningen, The Netherlands.

- [21] Kollmeyer, R. C. 1965. Iceberg Deterioration. Interim Report, U. S. Coast Guard, Washington, D. C., pp. 41-64, Report No. 11.
- [22] Lever, J. H., Bass, D. W., Lewis, C.F.M., Klein, K., Diemand, D., and Dyke, M. 1991. Iceberg/seabed interaction events observed during the DIGS experiment. *Journal of Offshore Mechanics and Arctic Engineering*, ASME, Vol.113, pp.74-87.
- [23] Lewis, J. C. and Bennett, G. 1984. Monte Carlo calculations of iceberg draft changes caused by roll. *Cold Regions Science and Technology*, Vol. 10, pp. 1-10.
- [24] Morgan, V. I. And Budd, W. F. 1977. The distribution, movement and melt rates of Antarctic icebergs. Symposium on Iceberg Utilization, Iowa State University, Ames, pp.220-228.
- [25] Mountain, D. G. 1980. On predicting iceberg drift. *Cold Region Science and technology*, Vol. 1, pp. 273-282.
- [26] Neshtba, S. and Josberger, E. G. 1979. On the estimation of Antarctic iceberg melt rate. Iceberg Dynamics Symposium, St. John's Newfoundland, June 4-5.
- [27] Nye, J. F. and Potter, J. R. 1980. The use of catastrophe theory to analyse the stability and toppling icebergs. *Annals of Glaciology*, Vol. 1.
- [28] Pachner, Jaroslav 1984. Handbook of numerical analysis applications, McGRAW-HILL BOOK COMPANY, pp.4-20 – 4-24. (Runge-Kutta Methods).
- [29] Robe, R. Q. 1980. Iceberg drift and deterioration. In *Dynamics of snow and ice masses*. Colbeck, S.C. (ed.). pp.211-260.
- [30] Robe, R. Q. Maier, D. C., and Kollmeyer, R. C. 1977. Iceberg deterioration. *Nature*, Vol.267, pp.505-506.
- [31] Russell-Head, D. S. 1980. The Melting of Free-drifting Icebergs. *Annals of Glaciology*, Vol.1, pp.119-122.

- [32] Salvesen, N., Tuck, E. O. and Faltinsen, O. 1970. Ship Motions and Sea Loads. Trans. SNAME.
- [33] Smith, S. D. and Banke, E. G. 1983. The influence of winds, currents and towing forces on the drift of icebergs. Cold Regions Science and technology, Vol. 6, pp. 241-255.
- [34] US Coast Guard 2001, <http://www.uscg.mil>
- [35] Venkatesh, S., Murphy, D. J., and Wright, G. F. 1994. On the deterioration of icebergs in the marginal ice zone. Atmosphere-Ocean, Vol.32, No.2, pp.469-484.
- [36] Venkatesh, S., El-Tahan, M., and Mitten, P. T. 1985. An Arctic iceberg deterioration field study and model simulations. Annals of Glaciology, Vol.6, pp. 195-199.
- [37] Venkatesh, S. and El-Tahan, M. 1988. Iceberg life expectancies in the Grand Banks and Labrador Sea. Cold Regions Science and Technology, Vol. 15, pp. 1-11.
- [38] Weeks, W. F. and Mellor, M. 1977. Some elements of iceberg technology. Proceedings Iceberg Utilization, A.A.Husseiny (ed.), Pergamon Press, pp. 45-98.
- [39] White, F. M.; Spaulding, M. L. and Gominho, L. 1980. Theoretical estimates of the various mechanisms involved in iceberg deterioration in the open ocean environment. U.S. Coast Guard Rep. No. CG-D-62-80, Wash, D.C., 126pp.
- [40] Witz, J. A. and Patel, M. H. 1984. A pressure integration for hydrostatic analysis. The Royal Institution of Naval Architects, pp. 285-294.
- [41] Zeeman, E. C. 1977. A catastrophe model for the stability of ships. In Catastrophe theory. Selected papers, 1972-1977. Reading Mass., Addison Wesley: 441-493 (Paper 17).

Appendix A

A-1 Runge-Kutta method

In this thesis, second Runge-Kutta method is used to solve motion equation. This is an initial value problem, that is to say, its initial conditions are known. The fundamentals of the method are described below. More details can be found in Pachner (1984). To solve the iceberg motion equation in Eqn. (3.48), the Runge-Kutta method is applied to approximate the values $\eta_i(t_n)$ at some time t_n , which is a time interval Δt past the time t_{n-1} at which the values $\eta_i(t_{n-1})$ are known.

The Runge-Kutta method is a numerical iterative procedure to solve the equations. Here we just pick up two continues time t_n and t_{n-1} to deduce the general expression which can be used in the program. The auxiliary coefficients of Runge-Kutta method are denoted as follows.

$$k_{i1} = \Delta t f_i[F(x_{n-1}, y_{n-1}, z_{n-1}, \phi_{n-1}, \theta_{n-1}, \psi_{n-1}), \dot{x}_{n-1}, \dot{y}_{n-1}, \dot{z}_{n-1}, \dot{\phi}_{n-1}, \dot{\theta}_{n-1}, \dot{\psi}_{n-1}] \quad (\text{A.1})$$

$$\begin{aligned}
\dot{k}_{12} = \Delta t f_1 [& F(x_{n-1} + \frac{1}{2} \Delta t \dot{x}_{n-1} + \frac{1}{8} \Delta t \dot{k}_{11}, y_{n-1} + \frac{1}{2} \Delta t \dot{y}_{n-1} + \frac{1}{8} \Delta t \dot{k}_{11}, z_{n-1} + \frac{1}{2} \Delta t \dot{z}_{n-1} + \frac{1}{8} \Delta t \dot{k}_{11}, \\
& \phi_{n-1} + \frac{1}{2} \Delta t \dot{\phi}_{n-1} + \frac{1}{8} \Delta t \dot{k}_{11}, \theta_{n-1} + \frac{1}{2} \Delta t \dot{\theta}_{n-1} + \frac{1}{8} \Delta t \dot{k}_{11}, \psi_{n-1} + \frac{1}{2} \Delta t \dot{\psi}_{n-1} + \frac{1}{8} \Delta t \dot{k}_{11}), \\
& \dot{x}_{n-1} + \frac{1}{2} k_{11}, \dot{y}_{n-1} + \frac{1}{2} k_{11}, \dot{z}_{n-1} + \frac{1}{2} k_{11}, \dot{\phi}_{n-1} + \frac{1}{2} k_{11}, \dot{\theta}_{n-1} + \frac{1}{2} k_{11}, \dot{\psi}_{n-1} + \frac{1}{2} k_{11}]
\end{aligned} \tag{A.2}$$

$$\begin{aligned}
\dot{k}_{13} = \Delta t f_1 [& F(x_{n-1} + \frac{1}{2} \Delta t \dot{x}_{n-1} + \frac{1}{8} \Delta t \dot{k}_{12}, y_{n-1} + \frac{1}{2} \Delta t \dot{y}_{n-1} + \frac{1}{8} \Delta t \dot{k}_{12}, z_{n-1} + \frac{1}{2} \Delta t \dot{z}_{n-1} + \frac{1}{8} \Delta t \dot{k}_{12}, \\
& \phi_{n-1} + \frac{1}{2} \Delta t \dot{\phi}_{n-1} + \frac{1}{8} \Delta t \dot{k}_{12}, \theta_{n-1} + \frac{1}{2} \Delta t \dot{\theta}_{n-1} + \frac{1}{8} \Delta t \dot{k}_{12}, \psi_{n-1} + \frac{1}{2} \Delta t \dot{\psi}_{n-1} + \frac{1}{8} \Delta t \dot{k}_{12}), \\
& \dot{x}_{n-1} + \frac{1}{2} k_{12}, \dot{y}_{n-1} + \frac{1}{2} k_{12}, \dot{z}_{n-1} + \frac{1}{2} k_{12}, \dot{\phi}_{n-1} + \frac{1}{2} k_{12}, \dot{\theta}_{n-1} + \frac{1}{2} k_{12}, \dot{\psi}_{n-1} + \frac{1}{2} k_{12}]
\end{aligned} \tag{A.3}$$

$$\begin{aligned}
\dot{k}_{14} = \Delta t f_1 [& F(x_{n-1} + \Delta t \dot{x}_{n-1} + \frac{1}{2} \Delta t \dot{k}_{13}, y_{n-1} + \Delta t \dot{y}_{n-1} + \frac{1}{2} \Delta t \dot{k}_{13}, z_{n-1} + \Delta t \dot{z}_{n-1} + \frac{1}{2} \Delta t \dot{k}_{13}, \\
& \phi_{n-1} + \Delta t \dot{\phi}_{n-1} + \frac{1}{2} \Delta t \dot{k}_{13}, \theta_{n-1} + \Delta t \dot{\theta}_{n-1} + \frac{1}{2} \Delta t \dot{k}_{13}, \psi_{n-1} + \Delta t \dot{\psi}_{n-1} + \frac{1}{2} \Delta t \dot{k}_{13}), \\
& \dot{x}_{n-1} + k_{13}, \dot{y}_{n-1} + k_{13}, \dot{z}_{n-1} + k_{13}, \dot{\phi}_{n-1} + k_{13}, \dot{\theta}_{n-1} + k_{13}, \dot{\psi}_{n-1} + k_{13}]
\end{aligned} \tag{A.4}$$

Each time, when we calculate the buoyancy of the model, we should transform the displacements and angles from body system to space system.

$$\begin{Bmatrix} X \\ Y \\ Z \end{Bmatrix} = \mathbf{T}^{-1} \begin{Bmatrix} x \\ y \\ z \end{Bmatrix} \tag{A.5}$$

where $\mathbf{T}^{-1} = \mathbf{T}_0^{-1} \mathbf{T}_1^{-1} \dots \mathbf{T}_{n-1}^{-1} \mathbf{T}_n^{-1}$

Finally,

$$\eta_i = \eta_{n-1} + \Delta t (\dot{\eta}_{n-1} + \frac{k_{i1} + k_{i2} + k_{i3}}{6}) \quad (\text{A.6})$$

$$\dot{\eta}_i = \dot{\eta}_{n-1} + \frac{k_{i1} + 2k_{i2} + 2k_{i3} + k_{i4}}{6} \quad (\text{A.7})$$

Appendix B

B-1 Flow charts of the STABLE

Main flow chart

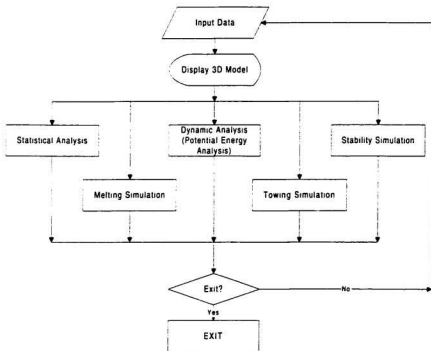


Figure B-1 Main flow chart of program STABLE

Statistical analysis section

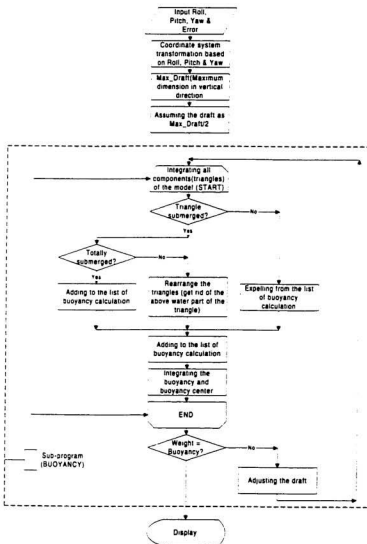


Figure B-2 Flowchart of the statistical analysis section

Potential energy analysis section

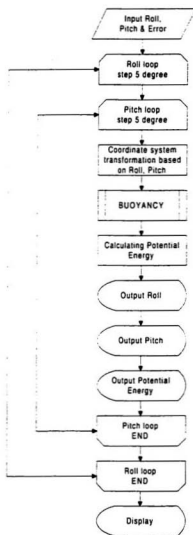


Figure B-3 Flowchart of potential energy analysis section

Motion simulation section

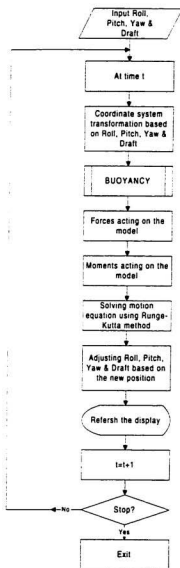


Figure B-4 Flowchart of motion simulation section

Towing and drag simulation section

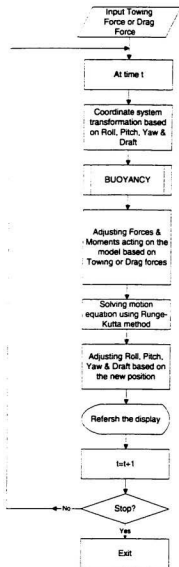


Figure B-5 Flow chart of towing and drag forces simulation section

Appendix C

C-1 A SLA format sample file

A 10m×10m×10m box stored in SLA format is listed as follows.

```
solid OBJECT
facet normal 0.000000e+000 0.000000e+000 -1.000000e+000
  outer loop
    vertex -5.000000e+000 -5.000000e+000 -5.000000e+000
    vertex 5.000000e+000 5.000000e+000 -5.000000e+000
    vertex 5.000000e+000 -5.000000e+000 -5.000000e+000
  endloop
endfacet
facet normal 0.000000e+000 0.000000e+000 -1.000000e+000
  outer loop
    vertex 5.000000e+000 5.000000e+000 -5.000000e+000
    vertex -5.000000e+000 -5.000000e+000 -5.000000e+000
    vertex -5.000000e+000 5.000000e+000 -5.000000e+000
  endloop
endfacet
facet normal 0.000000e+000 0.000000e+000 1.000000e+000
  outer loop
    vertex -5.000000e+000 -5.000000e+000 5.000000e+000
    vertex 5.000000e+000 -5.000000e+000 5.000000e+000
    vertex 5.000000e+000 5.000000e+000 5.000000e+000
  endloop
endfacet
facet normal 0.000000e+000 0.000000e+000 1.000000e+000
  outer loop
    vertex 5.000000e+000 5.000000e+000 5.000000e+000
    vertex -5.000000e+000 5.000000e+000 5.000000e+000
    vertex -5.000000e+000 -5.000000e+000 5.000000e+000
  endloop
endfacet
facet normal 0.000000e+000 -1.000000e+000 0.000000e+000
  outer loop
    vertex -5.000000e+000 -5.000000e+000 -5.000000e+000
    vertex 5.000000e+000 -5.000000e+000 -5.000000e+000
    vertex 5.000000e+000 -5.000000e+000 5.000000e+000
```

```

endloop
endfacet
facet normal 0.000000e+000 -1.000000e+000 0.000000e+000
  outer loop
    vertex 5.000000e+000 -5.000000e+000 5.000000e+000
    vertex -5.000000e+000 -5.000000e+000 5.000000e+000
    vertex -5.000000e+000 -5.000000e+000 -5.000000e+000
  endloop
endfacet
facet normal 1.000000e+000 0.000000e+000 0.000000e+000
  outer loop
    vertex 5.000000e+000 -5.000000e+000 -5.000000e+000
    vertex 5.000000e+000 5.000000e+000 -5.000000e+000
    vertex 5.000000e+000 5.000000e+000 5.000000e+000
  endloop
endfacet
facet normal 1.000000e+000 0.000000e+000 0.000000e+000
  outer loop
    vertex 5.000000e+000 5.000000e+000 5.000000e+000
    vertex 5.000000e+000 -5.000000e+000 5.000000e+000
    vertex 5.000000e+000 -5.000000e+000 -5.000000e+000
  endloop
endfacet
facet normal 0.000000e+000 1.000000e+000 0.000000e+000
  outer loop
    vertex 5.000000e+000 5.000000e+000 -5.000000e+000
    vertex -5.000000e+000 5.000000e+000 -5.000000e+000
    vertex -5.000000e+000 5.000000e+000 5.000000e+000
  endloop
endfacet
facet normal 0.000000e+000 1.000000e+000 0.000000e+000
  outer loop
    vertex -5.000000e+000 5.000000e+000 5.000000e+000
    vertex 5.000000e+000 5.000000e+000 5.000000e+000
    vertex 5.000000e+000 5.000000e+000 -5.000000e+000
  endloop
endfacet
facet normal -1.000000e+000 0.000000e+000 0.000000e+000
  outer loop
    vertex -5.000000e+000 5.000000e+000 -5.000000e+000
    vertex -5.000000e+000 -5.000000e+000 -5.000000e+000
    vertex -5.000000e+000 -5.000000e+000 5.000000e+000
  endloop
endfacet
facet normal -1.000000e+000 0.000000e+000 0.000000e+000

```



```
outer loop
  vertex -5.000000e+000 -5.000000e+000 5.000000e+000
  vertex -5.000000e+000 5.000000e+000 5.000000e+000
  vertex -5.000000e+000 5.000000e+000 -5.000000e+000
endloop
endfacet
endsolid OBJECT
```